AD-A168 300 TECHNIQUES FOR MICROWAVE DIELECTRIC MEASUREMENTS(U) 1/1
NAVAL WEAPONS CENTER CHINA LAKE CA D R GAGNON ET AL.
MAR 86 NWC-TP-6643 SBI-AD-E900 579

UNCLASSIFIED F/G 20/3 NL

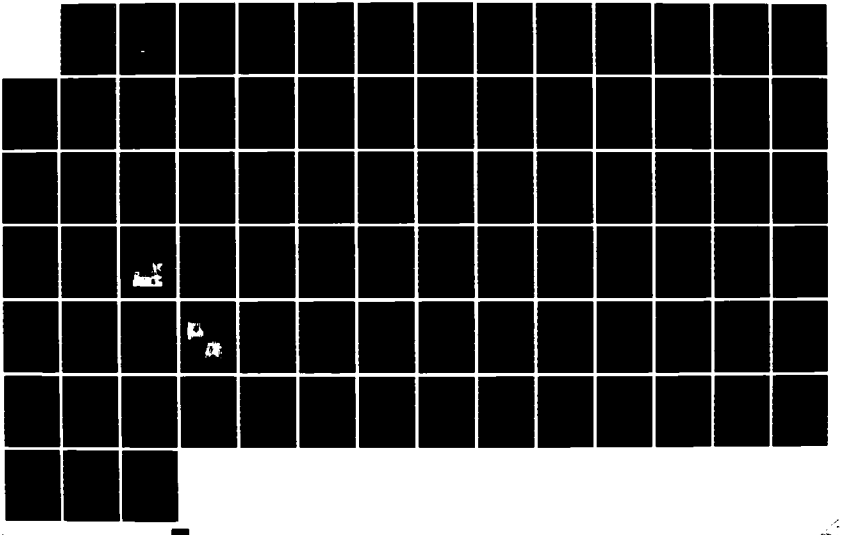

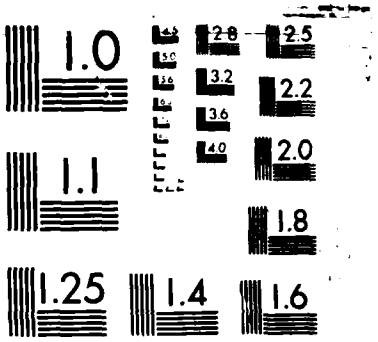

MICROCOPY RESOLUTION TEST CHART

NWC TP 6643

Techniques for Microwave Dielectric Measurements

by
D. R. Gagnon
D. J. White
G. E. Everett
D. J. Banks
Research Department

MARCH 1986

NAVAL WEAPONS CENTER
CHINA LAKE, CA 93555-6001

Approved for public release; distribution is unlimited.

Naval Weapons Center

FOREWORD

This is a final report on work that was performed at the Naval Weapons Center (NWC) during fiscal years 1983 through 1985. The work was supported by 6.2 funds from Naval Air Development Center Materials Block Funding and by funds provided by NWC as a Management Support Item. This report is published for the purpose of describing the NWC techniques for measuring the electrical properties of microwave materials. It is intended as a guide for potential users of these facilities. Although this is a final report, the authors recognize that the methods described here can be improved and anticipate that this work shall continue.

This report has been reviewed for technical accuracy by R. J. Dinger.

Approved by
E. B. ROYCE
Head, Research Department
25 March 1986

Under authority of
K. A. DICKERSON
Capt., USN

Released for publication by
B. W. HAYS
Technical Director

NWC Technical Publication 6643

Published by . . . . . Technical Information Department
Collation . . . . . Cover, 43 leaves
First printing . . . . . 110 copies

UNCLASSIFIED

SECURITY CLASSIFICATION OF THIS PAGE

AD-A168300

REPORT DOCUMENTATION PAGE

1a REPORT SECURITY CLASSIFICATION UNCLASSIFIED	1b RESTRICTIVE MARKINGS
2a SECURITY CLASSIFICATION AUTHORITY	3 DISTRIBUTION/AVAILABILITY OF REPORT A Statement; unlimited distribution.
2b DECLASSIFICATION/DOWNGRADING SCHEDULE	
4 PERFORMING ORGANIZATION REPORT NUMBER(S) NWC TP 6643	5 MONITORING ORGANIZATION REPORT NUMBER(S)
6a NAME OF PERFORMING ORGANIZATION Naval Weapons Center 6b OFFICE SYMBOL (If applicable)	7a NAME OF MONITORING ORGANIZATION
6c ADDRESS (City, State, and ZIP Code) China Lake, CA 93555-6001	7b ADDRESS (City, State, and ZIP Code)
8a NAME OF FUNDING/SPONSORING ORGANIZATION Naval Weapons Center 8b OFFICE SYMBOL (If applicable)	9 PROCUREMENT INSTRUMENT IDENTIFICATION NUMBER
8c ADDRESS (City, State, and ZIP Code) China Lake, CA 93555-6001	10 SOURCE OF FUNDING NUMBERS See back of page PROGRAM ELEMENT NO: 62761N; PROJECT NO:; TASK NO: WF61542; WORK UNIT ACCESSION NO: 1321303

11 TITLE (Include Security Classification)
TECHNIQUES FOR MICROWAVE DIELECTRIC MEASUREMENTS (U)

12 PERSONAL AUTHOR(S)
Gagnon, D. R., White, D. J., Everett, G. E., and Banks, D. J.

13a TYPE OF REPORT	13b TIME COVERED	14 DATE OF REPORT (Year, Month, Day)	15 PAGE COUNT
Final	FROM 82 Oct TO 85 Sep	1986, March	84

16 SUPPLEMENTARY NOTATION

17 COSATI CODES			18 SUBJECT TERMS (Continue on reverse if necessary and identify by block number)
FIELD	GROUP	SUB-GROUP	Radomes, Electrical Permittivity, Magnetic Permeability, High-Temperature Dielectric Measurements, Waveguide Cavity
20	03		
14	02		

19 ABSTRACT (Continue on reverse if necessary and identify by block number)

To fulfill the need for accurate characterization of the properties of electromagnetic window materials at microwave and millimeter-wave frequencies, a number of different techniques have been applied in the development of facilities for dielectric measurements at the Naval Weapons Center. The instruments include an iris-coupled waveguide cavity and a waveguide moving-vane dielectometer for measurements in X-band. A 7-millimeter coaxial transmission line fixture is employed with an automatic network analyzer system for measurements of complex permittivity and permeability in X- and Ku-bands. A lens-focused free-space bridge is used for Ka-band measurements, and a Fabry-Perot resonator has been built for use in Ka-band and higher frequencies. The waveguide cavity and the free-space bridge have been used also for high-temperature dielectric measurements. Each system is described, advantages and disadvantages are discussed, and some examples of measured results are given.

20 DISTRIBUTION/AVAILABILITY OF ABSTRACT	21 ABSTRACT SECURITY CLASSIFICATION
☐ UNCLASSIFIED/UNLIMITED ☐ SAME AS RPT ☒ DTIC USERS	UNCLASSIFIED
22a NAME OF RESPONSIBLE INDIVIDUAL D. R. Gagnon	22b TELEPHONE (Include Area Code) 619-939-1416 / 22c OFFICE SYMBOL 3814

DD FORM 1473, 84 MAR 83 APR edition may be used until exhausted
All other editions are obsolete

SECURITY CLASSIFICATION OF THIS PAGE

*U.S. Government Printing Office 1985—607-047

UNCLASSIFIED

10. Source of funding numbers:

Some of this work was funded as a Naval Weapons Center Management Support Item (MSI), Work Unit No. 7381808.

CONTENTS

1

INTRODUCTION

This report covers millimeter and microwave dielectric measurement work performed at the Naval Weapons Center (NWC). The apparatus used for obtaining elevated temperatures and making the measurements is described, and the principles of operation are set forth along with the results for various materials.

Missiles are being required to fly at ever higher mach numbers in more severe flight profiles with consequent aerodynamic heating and potential flight erosion. To design and build a usable radome, it is necessary to know the properties--electrical, mechanical, and thermal--of materials used (or potentially useful) in radome construction at the temperatures encountered.

It is also expected that missile systems will operate at millimeter as well as at microwave wavelengths. Because of the wide variety of materials used (or potentially useful) for radome construction, at least some can be expected to show significant change in their dielectric properties over the millimeter-microwave frequency ranges.

The work reported here represents an effort to supply laboratory measurements of the complex dielectric constants of materials over both millimeter and microwave frequencies at temperatures that might be encountered in a missile flight.

No single measurement method appears suitable for the complete range--ceramics, plastics, laminates, fiber-reinforced teflons and epoxies, etc.--of proposed materials over such a wide frequency range. Differences in dielectric constant magnitude, loss tangents, coefficients of thermal expansion, machinability, availability, chemical decomposition rates, and end products at high temperatures seem to preclude this. In any case, microwave dielectric constant and loss tangent measurements are difficult enough, especially at high temperatures, with enough sources of error and uncertainties that it is important to have overlapping measurement methods to supply corroboration or to pinpoint discrepancies.

Millimeter and microwave dielectric properties measurement techniques can be divided into groups (Reference 1-1). Transmission line methods look at a wave incident on a sample, and the interaction of the wave with the sample is determined. For example, the complex reflection or transmission coefficient can be measured, or, as in the Massachusetts Institute of Technology (MIT) Radiation Laboratory measurements, the reflection from a sample backed by a short can be determined (References 1-2 through 1-4). If swept frequency measurements are made, the frequency separation between transmission maxima can be used to determine the real part of the dielectric constant since these maxima occur when the sample thickness is an integral number of half wavelengths in the material.

Geometries which employ a washer-shaped sample in a coaxial line, a slab across a waveguide cross section, or a flat panel located between waveguide horns (see Section 3) are all examples of transmission line methods (References 1-5, 1-6). They have the advantage of conceptual simplicity and seeming ease of implementation. They generally, however, have some problems in determining loss tangent in low-loss materials, since the wave, neglecting multiple reflections within the sample (which rapidly die off for the relatively low dielectric constants of radome materials), basically passes through the sample only once or twice. Therefore, the sample absorbs only a small fraction of the available power, and precise measurement of this quantity can be difficult. When making transmission measurements, as in the case of classical measurements at Brewsters angle, the wave passes through the sample only once since the boundary reflection coefficient is zero; unless very thick samples are available, this represents the least sensitivity to loss tangent.

These measurement problems involving sample losses can be alleviated where practicable by using sources which are stable with respect to frequency and power output or very thick samples, together with a careful accounting for extraneous effects such as residual reflections within the components of the measuring system and (for free-space bridges) wave-front curvature. It probably remains true that transmission-line-type measurements are best suited for medium- rather than low-loss material loss tangent determination. In the case of radome materials, it is also true that loss tangents up to 0.01 are generally considered acceptable and the precise value of much lower loss tangents is relatively unimportant since the effect on electromagnetic performance will be small.

Resonant cavity methods enclose the dielectric sample in a microwave resonator, filling some fraction (up to 100%) of the resonator volume (References 1-7, 1-8). The quantities measured are usually the resonant frequency or the change in resonant frequency and the cavity Q with the cavity empty and with the sample in place. Another possibility lies in slightly changing a resonator dimension with insertion of

the sample to maintain the resonant frequency constant. The dimension change can be used to determine dielectric constant.

There can also be problems with resonant cavity measurements. The sample filling most or all of the cavity volume is roughly equivalent to multiplying the cavity dimensions by the index of refraction. This will greatly increase the density of excitable modes for the higher dielectric constant materials. Of course, it is hoped that symmetry will rule out many of the unwanted modes; however, any inhomogeneity in sample dielectric properties can destroy this symmetry and bring about the unwanted coupling. Many radome materials, such as ceramics, composites, laminates, etc., turn out to be somewhat inhomogeneous because of variations in the manufacturing processes.

Another problem lies in the relation between the loss tangent and the cavity Q. For other than very low-loss materials, the cavity Q will be dominated by the dielectric Q (inverse loss tangent) and many radome materials have sufficient loss to reduce the measured Q below acceptable limits for accurate measurements. One can, as we did, only partially fill the resonator with dielectric. This raises the Q and the measurement accuracy but can make it difficult to relate the measured Qs to the actual dielectric loss tangent. This is basically because the field distribution in a partially dielectric-filled cavity can be very different from that in the empty resonator. So far, this is a problem we have not solved satisfactorily in our X-band partially filled rectangular cavity measurements.

Lumped element measurements form another measurement category (Reference 1-9). Here a sample small in dimension with respect to a wavelength is considered (perhaps with corrections) as a static capacitor. For example, a small dielectric disk terminating a coaxial line (Reference 1-10) or positioned in the gap in a re-entrant coaxial cavity (Reference 1-11) can be treated in this manner. Because of the restrictions on sample size and wavelength, such measurements are difficult at the higher frequencies and have been confined mostly to S-band and below.

Perturbation measurements are also employed (Reference 1-12). Here a small sample is inserted into a resonant cavity, and the shift in resonant frequency and change in Q are measured and related to the complex dielectric constant. The theory is developed on the premise that the electromagnetic (EM) fields are unchanged in form and only slightly perturbed. Such measurements are attractive when only small samples are available. They can also be attractive from the standpoint that in elevated temperature measurements only a small sample must be heated. As usual, there are some basic pitfalls and difficulties. If the sample is small enough to leave the form of the EM fields unaltered, then the shifts in resonant frequency and Q are small, which leads to measurement inaccuracies. On the other hand, if the

perturbation is large enough to give useful values of these shifts, the validity of the theory can come into doubt. It is also true that as the sample is made smaller, the tolerances on the accuracy of the sample dimensions become increasingly important and small dimensional errors can cause large errors in the measured complex permittivity.

Another problem can lie in the depolarization factor (Reference 1-13). Dielectric bodies in an external electric field set up internal dipole fields in opposition to the external field. In the case of a small sample in a microwave cavity, this will reduce the perturbation effects and hence the resonant frequency shift and change in Q. The depolarization effect is sample-shape and electric-field-direction dependent. Very long, thin needles with the field parallel to the long axis have depolarization factors approaching zero. Flat disks with the field perpendicular to the plane of the disk have factors approaching 1. Spheres have a depolarization factor of 1/3 [all in meter-kilogram-second (MKS) units].

The higher the dielectric constant of the sample being measured, the smaller the relative dielectric constant (apparent dielectric constant divided by the actual dielectric constant) and the less accurate the measurement. This problem can be at least partially overcome by a careful choice of sample geometry, cavity configuration and mode, and sample placement. The depolarization can also be accounted for in the perturbation mathematics, although the frequency measurement accuracy may not be sufficient to take advantage of this approach.

Cavity perturbation measurements are perhaps at their best in relative measurements (e.g., determining the complex dielectric constant at an elevated temperature relative to its room-temperature value) rather than the determination of absolute value.

This report covers our efforts to date using resonant cavities (the partially dielectric-filled, half-height rectangular X-band cavity and the 35-gigahertz Fabry-Perot open resonator) and the transmission line (flat panel between 35-gigahertz focusing horns) methods. This work is far from complete, and it is our intention and hope to pursue this effort until we can perform accurate millimeter and microwave material properties measurements on a wide range of materials over a sizeable temperature range.

REFERENCES

1-1. "High Frequency Dielectric Measurement," in Proceedings of a Tutorial Conference on Measurement of High Frequency Dielectric Properties of Materials, National Physical Laboratory, Teddington, U.K., 27-29 March 1972. J. Chamberlain and G. W. Chantry, eds. Place, IPC Science and Technology Press, Ltd., 1973.

1-2. B. A. Burdick, T. J. Lyon, and J. E. Pippin. "Measurements of Large Dielectric Constants and Loss Tangents at 35 Gc/s," IEEE Trans. Instrum. Control, Vol. IM-13 (1964), pp. 318-23.

1-3. E. S. Sabisky and H. J. Gerritsen. "Measurement of the Dielectric Constant of Rutile (TiO_2) at Microwave Frequencies Between 4.2° and 300°K," J. Appl. Phys., Vol. 33 (1962), pp. 1450-53.

1-4. University of Michigan Research Institute. A Graphical Method for Measuring Dielectric Constants at Microwave Frequencies, by C. B. Sharpe. Ann Arbor, Mich., Electronic Defense Group, Department of Electrical Engineering, 1959. (Technical Report No. 94.)

1-5. K. H. Breeden, J. B. Langley, and A. P. Sheppard. "Complex Permittivity Measurements at Millimeter Wavelengths," in Dielectric Materials, Measurements, and Applications Conference Publication No. 67, IEE London, July 1970.

1-6. I. Ye Arsayev. "Effect of the Proximity of Receiving and Transmitting Antennas on the Measurement of Dielectric Constant of a Substance," Radio Eng. Electron. Phys., Vol. 15 (1970), pp. 1806-14.

1-7. Dielectric Materials and Applications, A. R. Von Hippel, ed. New York, John Wiley and Sons, Inc., 1954. Pp. 70-71.

1-8. R. N. Clark and C. B. Rosenberg. "Fabry-Perot and Open Resonators at Microwave and Millimetre Wave Frequencies, 2-300 GHz," J. Phys. E: Sci. Instrum., Vol. 15 (1982), pp. 9-24.

1-9. Dielectric Materials and Applications, A. R. Von Hippel, ed. New York, John Wiley and Sons, Inc., 1954. Pp. 47-62.

1-10. Dielectric Materials and Applications, A. R. Von Hippel, ed. New York, John Wiley and Sons, Inc., 1954. P. 69.

1-11. A. Kaczkowski and A. Milewski. "High-Accuracy Wide-Range Measurement Method for Determination of Complex Permittivity in Reentrant Cavity: Part A - Theoretical Analysis of the Method," Microwave Theory Tech., Vol. MTT-28 (1980), pp. 225-28; Part B - Experimental Analysis of Measurement Errors," ibid., pp. 228-31.

1-12. G. Birnbaum and J. Franeau. "Measurement of the Dielectric Constant and Loss of Solids and Liquids by a Cavity Perturbation Method," J. Appl. Phys., Vol. 20 (1949), p. 817.

1-13. C. Kittel. Introduction to Solid State Physics, 3rd ed. New York, John Wiley and Sons, Inc., 1966. P. 378.

2

THE PARTIALLY DIELECTRIC-FILLED X-BAND RECTANGULAR CAVITY

This measurement approach employs an X-band rectangular transmission cavity, as shown in Figure 2-1. Cavity coupling was through circular irises at each end, as shown in Figure 2-2. A thermocouple embedded in the cavity wall provides an input to a temperature controller that adjusts the oven current to maintain the desired oven-sample temperature.

The cavity is slid into a square (X-band flange size) channel from the ends of the cylindrical oven, and long stainless-steel waveguide sections are used for thermal isolation on either side of the cavity. This oven is capable of increasing the cavity and sample temperatures to 800°F. In order to avoid long line effects from the inevitable minor reflections from the waveguide-coaxial transitions, etc., a rotary vane attenuator was placed at the stainless-steel waveguide inputs to provide isolation or padding.

A receiver (either a Pacific Measurements scalar analyzer or a Scientific Atlanta receiver with a chart recorder) was used to determine the cavity output magnitude versus frequency. This shows the resonances with their frequencies and Qs.

Our initial efforts employed a simple half-wavelength cavity made from a short section of standard WR-90 X-band waveguide. This brought about several problems. We were attempting to measure a large variety of materials (ceramics, plastics, epoxies, laminates, composites, mixtures, etc.), and many were lossy enough to lower the Q below that necessary for good measurements. In other words, good sharp cavity resonances on which to base the calculations could not be obtained.

The high mode density was also a serious problem. The dielectric constant calculated from the resonant frequency and the dimensions of the dielectric-filled cavity is

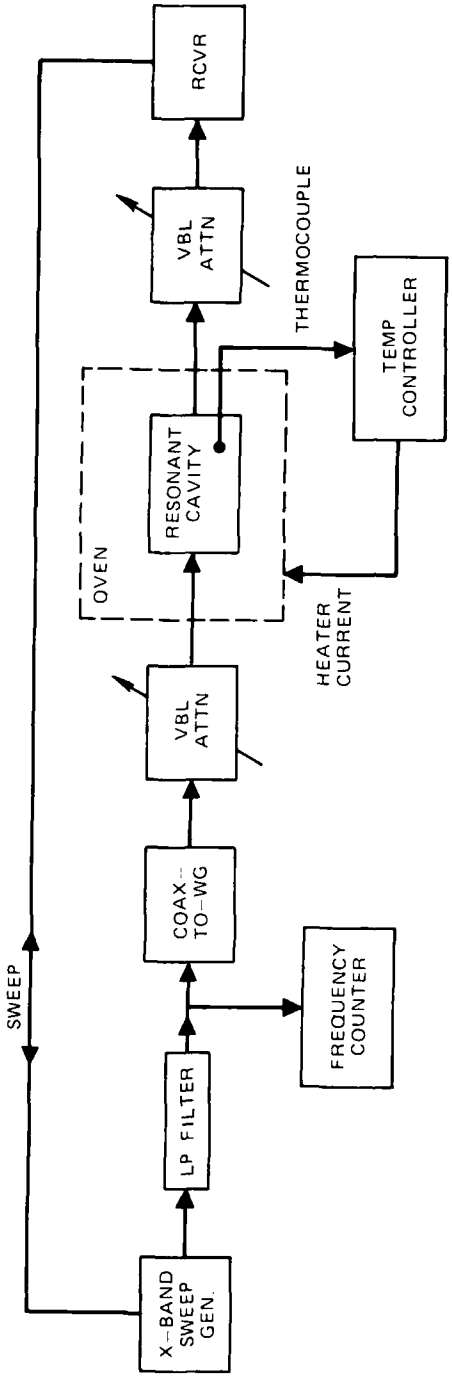

FIGURE 2-1. Generalized Block Diagram of X-Band Rectangular Cavity Measurement Setup.

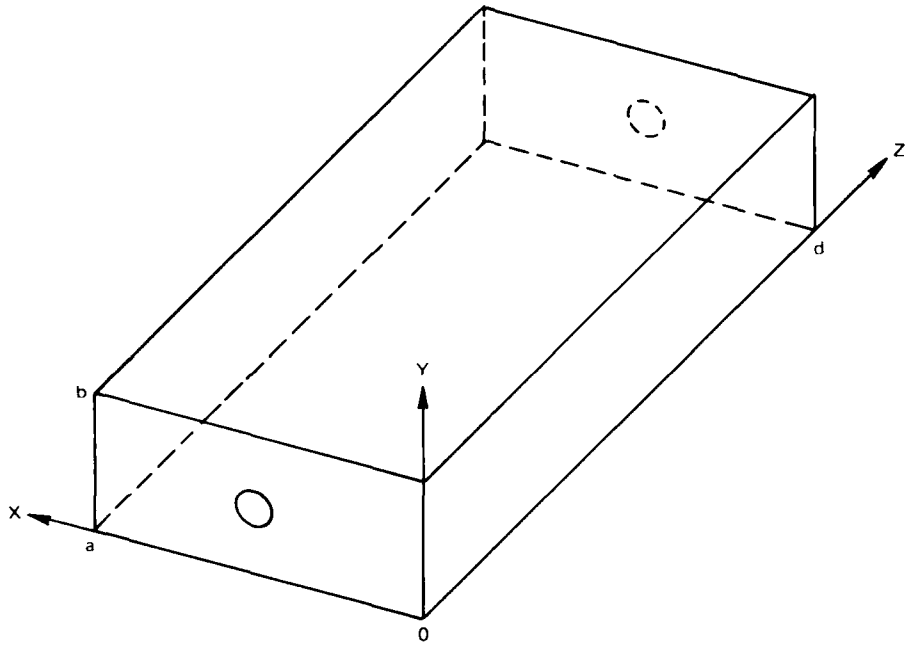

FIGURE 2-2. Rectangular Transmission Cavity of Dimensions a,b,d With Circular Coupling Irises and Coordinate System.

$$\varepsilon' = \left(\frac{c}{2f_o}\right)^2 \left[\left(\frac{m}{a}\right)^2 + \left(\frac{n}{b}\right)^2 + \left(\frac{p}{d}\right)^2\right] \qquad (2\text{-}1)$$

where c is the velocity of light in a vacuum; f_o is the resonant frequency; a,b,d are the cavity width, height, and length, respectively, while m,n,p are integers representing the mode order (number of equivalent half-wavelengths in the x,y,z directions).

Empty, the cavity resonated in the TE_{101} mode at resonant frequency f_e. Filled with dielectric, however, the 101 resonance drops to

$$f_o = \frac{f_e}{\sqrt{\varepsilon'}} \qquad (2\text{-}2)$$

Since most radome materials have $\varepsilon' > 2$, filling the cavity with dielectric moved the 101 mode out of band while bringing the 102 mode

within band. Unfortunately, it also brings others such as the TE_{201}, TE_{111}, and TM_{111} modes within band (8 to 12 gigahertz).

The cavity symmetry was such that normally most of these modes (excluding the TE_{102}) should not be excited. Unfortunately, many of the materials being measured were not strictly homogeneous (ceramics, experimental composites, mixtures), and the extraneous modes did sometimes appear, apparent symmetry notwithstanding.

A third difficulty involved the coupling irises. Equations such as Equation 2-1 are derived on the assumption of perfectly conducting cavity walls. Coupling into the cavity is usually accounted for by assuming a cavity equivalent resonant lumped circuit with perfect transformers supplying the coupling. Actually, an iris appears to supply some shunt susceptance across the cavity, lowering the resonant frequency. This, in turn, implies that the electrical cavity length is somewhat greater than its actual physical length. Another, more exact, way of treating this problem is to observe that a single mode cannot be used to match exactly the boundary conditions at the end walls containing the irises. Instead, the lowest order mode plus an infinite sum of higher order modes are required theoretically, although this sum can be terminated at some point for all practical purposes. If the higher order modes are below cutoff, they are evanescent and decay exponentially away from the iris in the propagation direction.

Using this approach, it is easy to see that the presence of the dielectric raises the cutoff frequency of all modes; hence, the coupling will be altered. In addition, some modes are no longer evanescent and thus are able to propagate the length of the cavity. That is, the coupling coefficients of the empty and filled cavities are different; thus, they have some effect on the cavity equivalent electrical length and introduce error in the calculated dielectric constant. This has a much more severe effect on the loss tangent measurements, since the measured (loaded) Q is a strong function of the coupling coefficient as well as of the dielectric and cavity wall losses.

A fourth set of problems was encountered in the high-temperature measurements. Measurements in the TE_{mop} modes require a close sample fit, particularly in the y- or b-direction. The differential thermal expansion, particularly between the plastic and Teflon-based samples and the metal cavity, lead to sample warping, extrusion, cracking, and crumbling.

To deal with these problems, we went to a half-height (b = 0.2 inch instead of 0.4 inch in Figure 2-2) waveguide X-band cavity. This decreases substantially the number of possibly excited modes (mode density), as can be seen from Equation 2-1. The cavity was also lengthened to 2.5 inches. This does increase the overall mode density slightly, although not as severely as might be inferred from Equation 2-1, since the cutoff frequency of a rectangular waveguide is given by (Reference 2-1)

$$(f_c)_{mn} = \frac{\left[\left(\frac{m}{a}\right)^2 + \left(\frac{n}{b}\right)^2\right]^{1/2}}{2\sqrt{\epsilon'}} \tag{2-3}$$

and those modes which are below cutoff are not excited in any case. However, lengthening the cavity decreases the iris effects--the change in coupling in the presence of the dielectric. (While the iris still increases the electrical length of the cavity, this increase is a smaller percentage of the overall length leading to reduced error.)

The long cavity also allows several TE_{nop} resonances (TE_{103}, TE_{104}, and TE_{105} in the empty guide) to be examined across X-band (8 to 12 gigahertz). Mode index numbers can be assigned to each resonance and then varied until the calculated dielectric constant agrees for all of them. The dielectric ambiguity is thereby removed because of the difference in phase velocity for each mode in a guided-wave structure. This assumes a dispersionless dielectric, which is usually the case across a single-microwave band for typical radome materials.

Finally, the cavity was only partially dielectric filled. The dielectric occupied a cross section, as shown in Figure 2-3. The configuration of Figure 2-3(a), with a dielectric slab centered lengthwise down the long dimension of the cavity, is used primarily for accurate room-temperature measurements. The TE_{mop} modes are employed, and for the odd modes the transcendental equation to be solved is

$$\tan d_2\sqrt{(\omega_o/3)^2 - (p\pi/d)^2}\ \tan d_1\sqrt{\epsilon'(\omega_o/3)^2 - (p\pi/d)^2}$$

$$= \frac{\sqrt{1 - (3p/2f_o d)^2}}{\sqrt{\epsilon' - (3p/2f_o d)^2}} \tag{2-4a}$$

and for the even modes

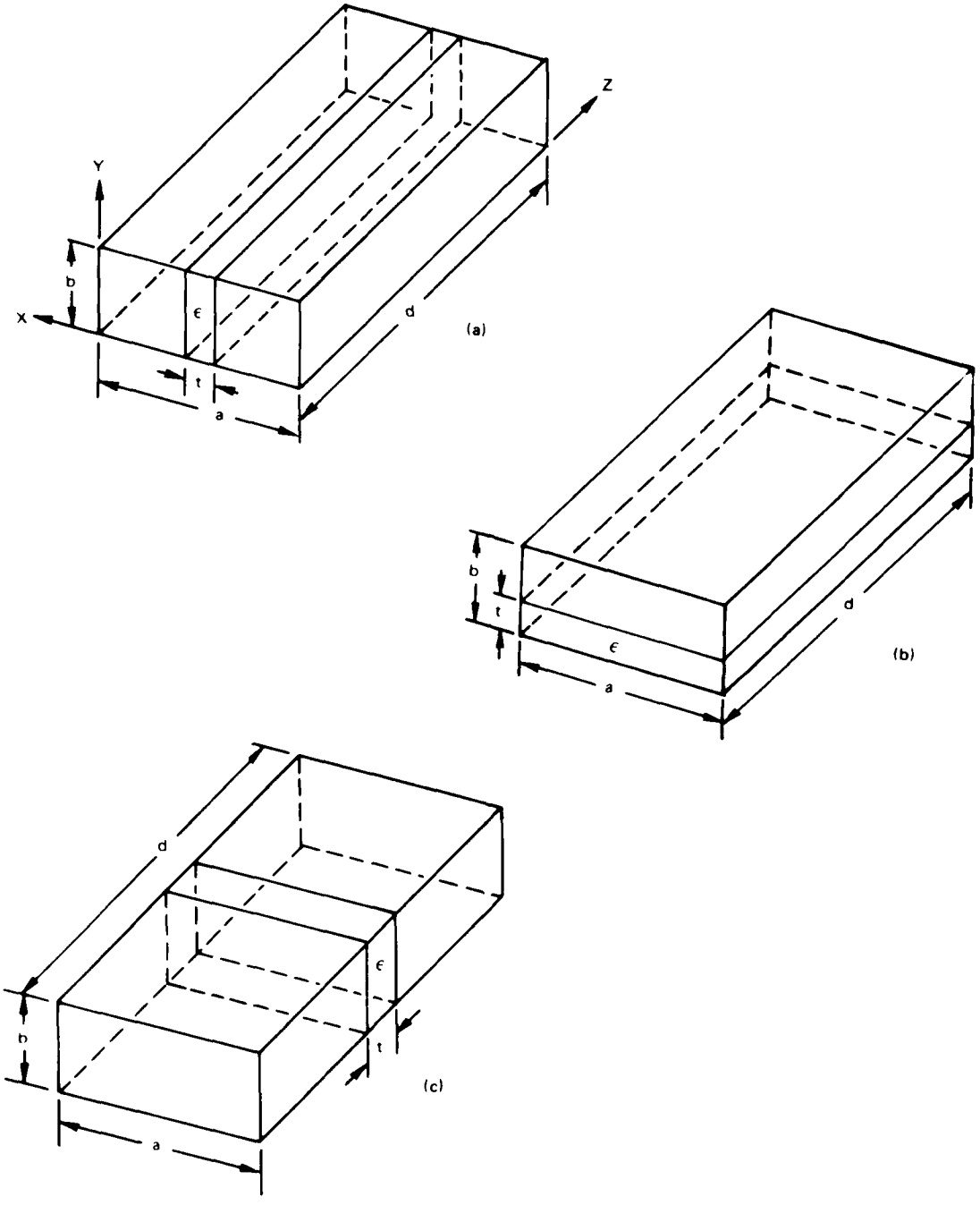

FIGURE 2-3. Various Ways of Partially Filling the Rectangular Cavity With Dielectric for Which Transcendental Equations Can Be Solved Readily for Transverse Electric (TE), Longitudinal Section Electric (LSE), and Longitudinal Section Magnetic (LSM) Modes.

$$\sqrt{1 - (3p/2f_o d)^2} \tan d_1\sqrt{\varepsilon(\omega_o/3)^2 - (p\pi/d)^2}$$

$$= - \sqrt{\varepsilon' - (3p/2f_o d)^2} \cdot \tan d_2\sqrt{(\omega_o/3)^2 - (p\pi/3)^2} \quad (2\text{-}4b)$$

where $d_1 = t/2$ (one-half the thickness of the sample) and $d_2 = (a-t)/2$. $\omega_o = 2f_o$, and f_o is given in tens of gigahertz (i.e., 10 gigahertz means $f_o = 1.0$ in these units).

The integer p specifies the number of half-waves along the length d of the cavity. The index m is determined by the root of the transcendental equation. The smallest value of ε in Equation 2-4a is at m = 1; the next value is found at m = 3, and so on. The even values come from the roots of Equation 2-4b. The m = 1 root is roughly analogous to a single half-wavelength across the width of the cavity. The m = 2 root from Equation 2-4b corresponds to a full wave, etc. The even modes are suppressed by the symmetry of the situation, while the higher order modes (m = 3, etc.) are below cutoff for reasonable choice of thickness t and dielectric constant in the range of typical radome materials. The index for the height b is kept to zero by the half-height. Thus, only the TE_{10p} modes are normally dealt with.

For the elevated temperature measurements, LSM modes were employed with configuration (b) of Figure 2-3. This configuration allows free sample expansion in the y-direction, while clearance can be provided at the sample edges for thermal growth in the x- and z-directions. The electric field close to the cavity walls is small since the tangential electric field must go to zero there; hence, the effect of the clearances at the sample edges should be negligible. This was confirmed by measurements on a sample of known dielectric constant, first as a tight fit and then after trimming to give clearance.

The transcendental equation to be solved for the LSM mode case is (Reference 2-2)

$$\sqrt{k_o^2\varepsilon - (N/a)^2 - (p/d)^2} \tan t\sqrt{k_o^2\varepsilon - (N/a)^2 - (p/d)^2}$$

$$= - \varepsilon\sqrt{k_o^2 - (N/a)^2 - (p/d)^2}$$

$$\cdot \tan (b-t)\sqrt{k_o^2 - (N/a)^2 - (p/d)^2} \quad (2\text{-}5)$$

Here, $k_o = 2\pi/\lambda_o$, or in terms of the tens of gigahertz units of Equation 2-4, $\omega'_o/3$.

It should be pointed out as a pitfall that for sufficient sample thickness combined with dielectric constant and frequency, the microwave energy can become "trapped" in the dielectric. The field exterior to the dielectric then decays exponentially or becomes evanescent. This takes place whenever

$$\left(\frac{n\pi}{a}\right)^2 + \left(\frac{p\pi}{d}\right)^2 > k_o^2 \tag{2-6}$$

(The thickness enters in through k_o, since the greater the dielectric loading, the lower the resonant frequency, and the smaller k_o). In such cases, Equations 2-4 and 2-5 can be rewritten using the following relation:

$$\tan jx = j \tan h\, x \tag{2-7}$$

Equations 2-4a and 2-4b become

$$\tan h\, d_2\sqrt{(p\pi/d)^2 - (\omega'_o/3)^2}\ \tan d_1\sqrt{\varepsilon'(\omega'_o/3)^2 - (p\pi/d)^2}$$

$$= \frac{\left(\sqrt{(3p/2f_o d)^2 - 1}\right)}{\sqrt{\varepsilon' - (3p/2f_o d)^2}} \tag{2-8a}$$

and

$$\sqrt{(3p/2f_o d)^2 - 1}\ \tan d_1\sqrt{\varepsilon'(\omega_o/3)^2 - (p\pi/d)^2}$$

$$= -\sqrt{\varepsilon' - (3p/2f_o d)^2}\ \tan h\, d_2\sqrt{(\omega_o/3)^2 - (p\pi/d)^2} \tag{2-8b}$$

while Equation 2-5 becomes

$$\sqrt{k_o^2\varepsilon' - (N\pi/a)^2 - (p\pi/d)^2}\ \tan\ t\sqrt{k_o^2\varepsilon - (N\pi/a)^2 - (p\pi/d)^2}$$

$$= \varepsilon'\sqrt{(N\pi/a)^2 + (p\pi/d)2 - k_o^2}$$

$$\tan\ h(b-t)\sqrt{(N\pi/a)^2 + (p\pi/d)^2 - k_o^2} \qquad (2\text{-}9)$$

Some work was done with the configuration of Figure 2-3(c), particularly where only short samples were available. Assuming the sample is centered lengthwise, then Equations 2-4(a) and 2-4(b) or, in the case of trapped waves, Equations 2-8(a) and 2-8(b) can be used directly by interchanging the dimensions "a" and "d." Of course, the integer p will differ as there will usually be only one or two spatial variations along "a" (being just the guide width), whereas there will be several along "d." It follows that usually not only the index p be 1 or 2 in configuration (c) in Figure 2-3, but the argument of the tangent term will be of higher order (e.g., between π and $3\pi/2$ for an odd solution). In configuration (a) of Figure 2-3, however, p will be some integer greater than 2 to 3, and the lowest order argument (between zero and $\pi/2$, which means only the odd-mode solution need be used) for the tangent will yield the appropriate dielectric constant.

It is interesting to note that the configuration of Figure 2-3(c) can be analyzed directly by signal flow graph techniques, whereas this does not appear to be the case in Figure 2-3(a). Work still is to be done to reconcile the apparently different expressions obtained for Figure 2-3(c) from signal flow graph analysis and the consideration of the modes in a partially dielectric-loaded resonator with perfectly conducting walls. This comparison could be of importance in both error analysis for this type of measurement and in understanding the effects of coupling and direction of energy propagation on a cavity resonance.

Some measurements were also taken in other configurations; for example, those similar to Figures 2-3(a) and (c), where the dielectric slab was not centered, or the use of two long samples along the waveguide walls. Such configurations might have particular applications. For example, placing the sample next to a side wall in the TE_{mop} mode ensures minimum electric field in the sample and, thus, a smaller shift in the resonant frequency. This could be useful in measuring the properties of high dielectric constant materials where it is not desirable to make a very thin sample.

Some measurements were also made using the TE_{10p} circular waveguide cavity loaded with a dielectric disk. The transcendental

equations to be solved are very similar to those of the dielectric-loaded rectangular cavity. This approach needs more development (for example, the residual frequency modulation (FM) from our sweepers made it difficult to obtain clean resonances because of the very high Qs of TE_{10p} cavities) but does have promise. For example, the electric field lines in the TE_{10} circular waveguide mode are closed loops that go to zero at the walls. This means very low wall losses and very high intrinsic Q. It also means that a sizeable gap between the dielectric sample disk and the cavity is of little consequence since the electric field is negligible there.

Determining the dielectric loss tangent for the partially dielectric-filled cavity remains an unfinished problem. The difficulty arises because of the differences in field configurations between the partially filled and the empty cavity. In a completely filled cavity, the field configuration basically is unaltered from that of the empty cavity; hence, the Q due to wall losses remains unchanged, and one can write the classic expressions such as (References 2-3, 2-4)

$$Q^{-1} = Q_e^{-1} + Q_d^{-1} \tag{2-10}$$

with a high degree of approximation. Here Q is the measured Q of the dielectric field cavity, Q_e the Q of the empty cavity, and Q_d the dielectric Q or reciprocal loss tangent. There are approximations in such an expression, a major one being that the presence of the dielectric does not appreciably alter the cavity coupling. The measured Q is related to the sources of loss: dielectric loss, wall loss, and losses through the coupling structures to the external circuitry.

The theoretical unloaded Q of a rectangular cavity with walls of known conductivity can readily be found for the lowest order modes as (Reference 2-5)

$$Q = \frac{\pi\eta}{4R_s} \cdot \frac{2b(a^2 + d^2)^{3/2}}{ad(a^2 + d^2) + 2b(a^3 + d)^3} = \frac{\eta K}{R_s} \tag{2-11}$$

where $\eta = \eta_o/\sqrt{\varepsilon}$ (the characteristic impedance of free space divided by the square root of the dielectric constant); R_s is the conductor surface resistance; a,b,d are the cavity dimensions; and K depends only on cavity geometry.

Unfortunately, this says the "Q" of a dielectric-filled cavity changes from the empty cavity even with a lossless dielectric, the ratio being

$$\frac{Q_e}{Q} = \frac{\sqrt{\epsilon} R_s}{R_{se}} \tag{2-12}$$

with

$$R_s = \frac{\sqrt{\pi f \mu}}{\sigma} \tag{2-13}$$

so that

$$\frac{R_s}{R_{se}} = \left(\frac{f_o}{f_{oe}}\right)^{1/2} = (\epsilon)^{-1/4} \tag{2-14}$$

It follows that

$$\frac{Q_e}{Q} = \epsilon^{1/4} \tag{2-15}$$

The effect given by Equation 2-15 seems to be commonly ignored in the usual application of Equation 2-10, and we have to wonder, in terms of absolute accuracy, how good many of the reported loss tangents measured in resonant systems really are!

It seems that Equation 2-10 should actually relate the measured Q of a dielectric-filled cavity to the dielectric Q_d (reciprocal loss tangent) and the Q of a cavity filled with a lossless dielectric with the same real part of the dielectric constant, at least for low-loss materials. That is, Q_e^{-1} in Equation 2-10 should be multiplied by $\epsilon^{1/4}$.

Considering such pitfalls as illustrated in the foregoing discussion, the measurement of dielectric losses in the partially dielectric-filled rectangular cavity has further difficulties. The primary problem is that the field distributions are different in the dielectric-loaded and in the empty cavity; thus, there seems to be no

simple way to find the term in Q_c^{-1} (or $\varepsilon^{1/4}/Q_e$) from the real part of the dielectric constant and the empty cavity Q_e. One would need to measure an identical geometry of partially filled cavity with a lossless dielectric with the same real part--an approach that is not practical.

An iterative process might offer a solution. The real part of the dielectric constant could be calculated as if the material were lossless. This could be used to find the TE, LSE, of LSM field distribution. This is then integrated over the cavity walls to find the equivalent Q_e, with Q_d then calculated from Equation 2-10 or its actual experimental equivalent

$$Q^{-1} = Q_e^{-1} + Q_d^{-1} + Q_c^{-1} \tag{2-16}$$

where Q_c is the Q due to losses to the external circuit through the coupling apertures. (Q would then be the actual measured loaded Q.) Q_c perhaps could be obtained to sufficient accuracy by comparing the measured Q_e of the actual empty cavity with the theoretical empty Q as in Equation 2-11, assuming the coupling is independent of dielectric loading. Another approach would be to conceptually break the transcendental equations, such as 2-4, 2-5, 2-8, or 2-9, into real and imaginary parts with ε complex and attempt to solve these directly in terms of the experimental measurements.

The complexity of the problem perhaps can be underscored in the case of wave trapping, where the waves in the empty portions of the cavity become evanescent. The wall losses must then become vanishingly small in the empty part of the cavity, with the wall losses substantially confined to those parts of the walls in direct contact with the dielectric. In the case of a low-loss dielectric, the measured loaded Q could conceivably be larger than that of the empty cavity.

In summation, the problem of measuring accurate loss tangents has yet to be satisfactorily resolved for the partially dielectric-filled rectangular cavity and awaits further efforts.

EXPERIMENTAL RESULTS

Figure 2-4 illustrates the manner in which the data are reduced. The sample is inserted into the cavity and the resonant frequencies (four in this example) are measured across X-band. This example has the sample configuration of Figure 2-3(a). The transcendental

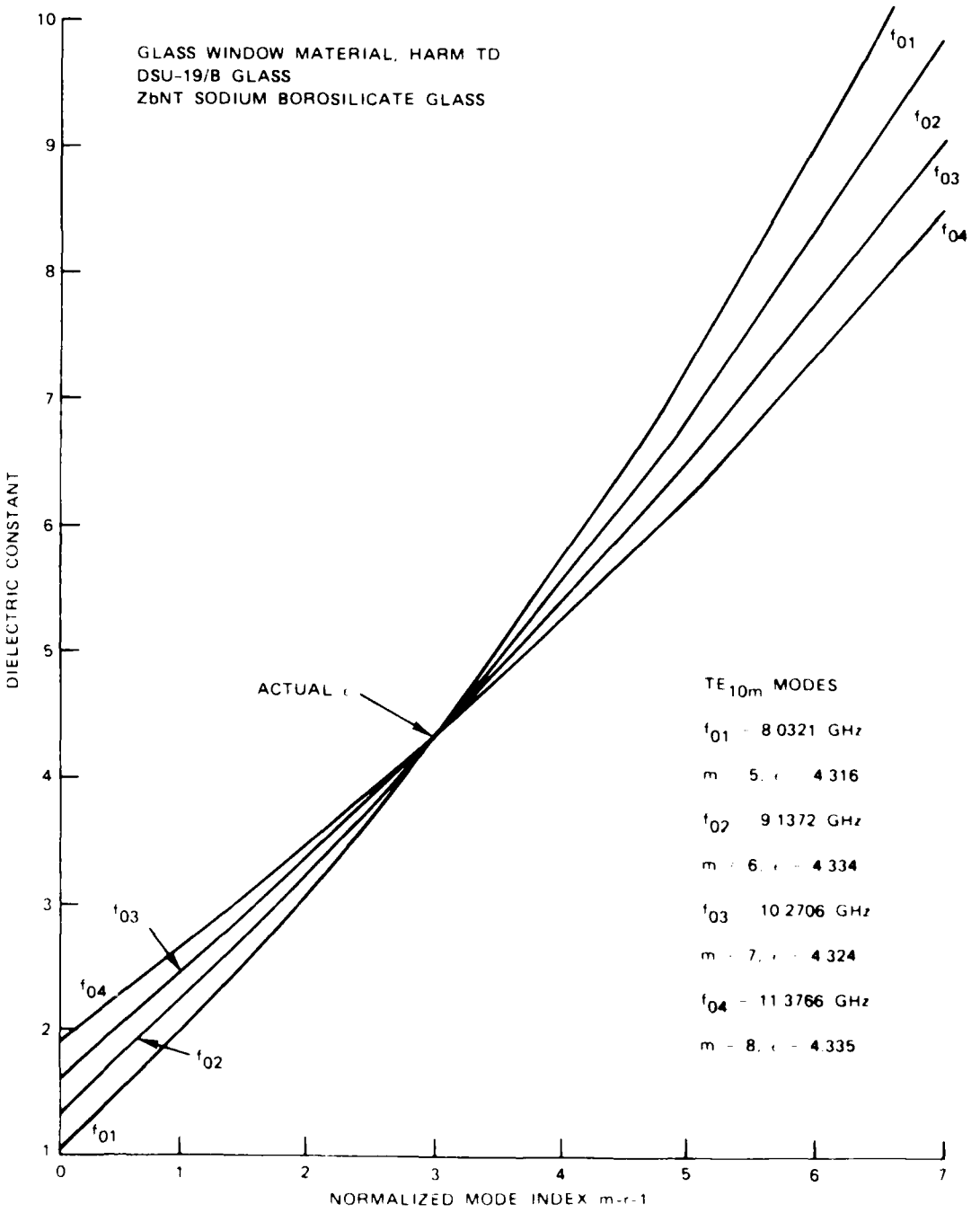

FIGURE 2-4. Calculated Dielectric Constant Versus Normalized Mode Index With Partially Dielectric-Filled Rectangular Cavity in TE_{10m} Mode.

Equations 2-4 or 2-8 are used along with the known cavity and sample dimensions to calculate the dielectric constant(s) for different numbers of half wavelengths m (expressed as p in the equations) along the cavity length. Figure 2-4 shows plots for each resonant frequency of the calculated dielectric constant versus a normalized index, where r is the order number of the resonant frequency: r = 1 for f_{01}, r = 2 for f_{02}, etc. In this example, the plots for the different resonant frequencies cross for m-r-1 = 3, and it follows that this is the correct unambiguous dielectric constant for this glass window material used in a high-speed antiradiation missile (HARM) application. The discrepancies (standard deviation 0.008) between the calculated values are due to various experimental errors, while the curvature in the plots is a result of waveguide dispersion.

This setup has been used to measure a large variety of materials. Some typical room-temperature results are given in Table 2-1.

TABLE 2-1. Representative Measured Dielectric Constants From Partially Dielectric-Filled Rectangular X-Band Cavity.

Material	Dielectric constant	Material source	Comments
Avcoat 8029	2.23	AVCO	For NWC, Code 3242. Contains reinforcing fibers; difficult to machine.
Teflon	2.05	Commercial	Control.
Laminate		Naval Air Development Center (NADC)	A. Lee, Code 60613, NADC. Very tough material; anisotropic; average.
SB-129 Propellant	7.50	NWC	Lossy; measurement accuracy poor.
Mullite Vat 21	5.86	Naval Research Laboratory (NRL)	Code 6360, NRL. Apparently homogeneous.
Space shuttle tile	1.14	Rockwell International Corp.	For NWC, Code 3522. Fragile; crumbles; pure SiO_2; 90% air.
Stycast HiK = 12	11.70	Emerson and Cummings	Control.

Anisotropic materials also play a role in radome construction, and this system can be used to measure such materials in the TE_{mop} modes provided the electric field is aligned along a principal axis of the dielectric. Some results of such measurements are given in Table 2-2.

TABLE 2-2. Representative Measured Dielectric Constants for Anisotropic Materials Using Partially Dielectric-Filled Rectangular X-Band Cavity.

Material	ε_x	ε_z
3M Company, 300 board	2.85	2.41
Rogers Corp., RT Duroid D05880 (17SKS)	2.19	2.29
NADC experimental laminate	3.07	2.66
Duroid 5870M	2.34	2.42

This method can be adapted to measure certain types of inhomogeneous materials by cutting several small samples and measuring the permittivity of each piece, using the configuration of Figure 2-3(c). Homogeneity is an important problem with radome and microwave dielectric materials, which are mixtures, laminates, fiber reinforced, or ceramic. Maintaining even distributions, desired volume fractions, and densities poses difficult problems. Table 2-3 gives some measured results on inhomogeneous materials. Omohundro Corporation products NAFA-5050 and NAFA-2575-1 are syntactic foams made using hollow alumina microspheres, while the lens material is a polyfoam filled with aluminum flakes. As in aluminum spray paint (at least the spray paints we have checked), the aluminum flakes are evidently coated with insulating materials to prevent flake-to-flake electrical contact. Careful visual examination indicated that the inhomogeneity was caused by an uneven distribution of the aluminum particles.

Finally, of course, the cavity can be used to measure dielectric properties at elevated temperatures up to 800°F in the LSM modes. Hindsight tells us that free-space methods are preferable for high-temperature measurements if a wide variety of materials is to be considered. If cavities (or waveguides) are to be used, the thermal expansion of both the sample and the waveguide or cavity must be considered, both from the electromagnetic and the structural points of view. A sample that warps or splits will probably invalidate the EM analysis, and one that deposits a chemical coating on a cavity interior

TABLE 2-3. Representative Measurements (Relative Dielectric Constant) of Inhomogeneous Materials.

Sample number	Omohundro NAFA-5050	Omohundro NAFA-2575-1	Microwave lens material
1	1.95	2.56	2.69
2	1.96	2.52	3.25
3	2.00	2.50	2.95
4	1.88	2.52	2.88
5	1.89	2.57	3.64
6	1.89	2.46	2.85
7	1.94	2.43	2.82
8	1.90	----	3.21
9	----	----	2.82
10	----	----	3.56
11	----	----	3.48
12	----	----	3.03
13	----	----	2.69
14	----	----	2.89
15	----	----	3.46
16	----	----	2.99
17	----	----	2.82
18	----	----	2.87
Average	1.93±0.04	2.51±0.05	3.05±0.31

will probably at least ruin the Q-value. For example, Figure 2-5 shows some measured results for Duroid 5870M. Here the dielectric constant is calculated from the cavity resonant frequencies, corrected for the thermal expansion of the cavity, as determined by experimental measurement of the resonant frequencies versus temperature. There are two curves: (1) dielectric constant calculated without including the sample thermal expansion and (2) decreasing dielectric constant with increasing temperature calculated with the sample thermal expansion.

In this case, the correction for the expansion of the beryllium-copper cavity is relatively insignificant compared to that brought about by the large thermal expansion coefficient of Duroid. The thermal expansion data used are shown in Figure 2-6. In this case, the reinforcing fibers lie in the plane of the sample, and the thermal expansion coefficient normal to the plane was used. In the case of materials with such a large thermal expansion, the calculated dielectric constant can be no better than the thermal expansion coefficient used. Figure 2-7 shows some data obtained from the Rogers Corporation for both 5650M and 5870M Duroids. While the curves of Figure 2-7(a)

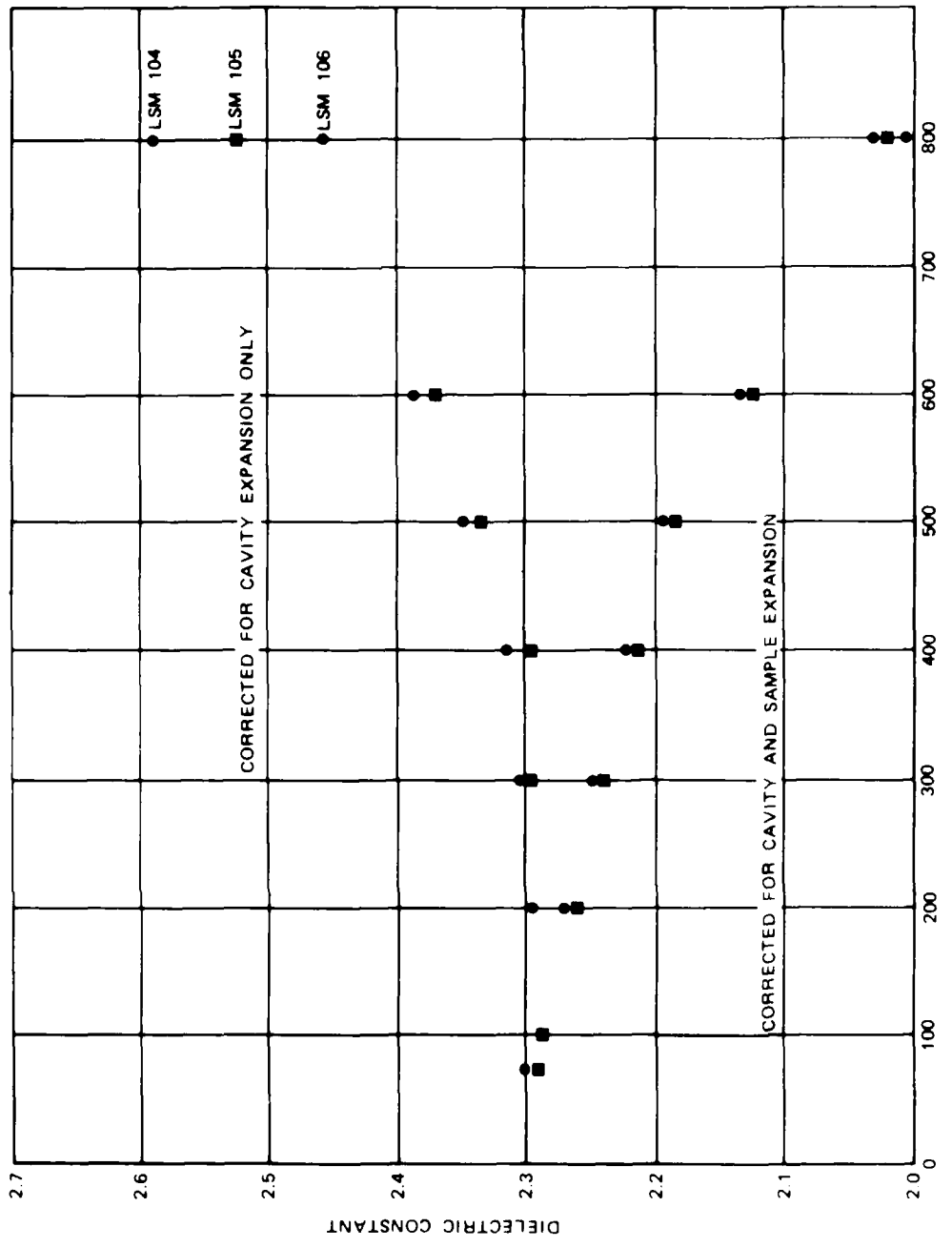

FIGURE 2-5. Dielectric Constant of Duroid 5870M Versus Temperature, Corrected and Uncorrected for Thermal Expansion of Sample But Corrected in Both Cases for Thermal Expansion of Cavity.

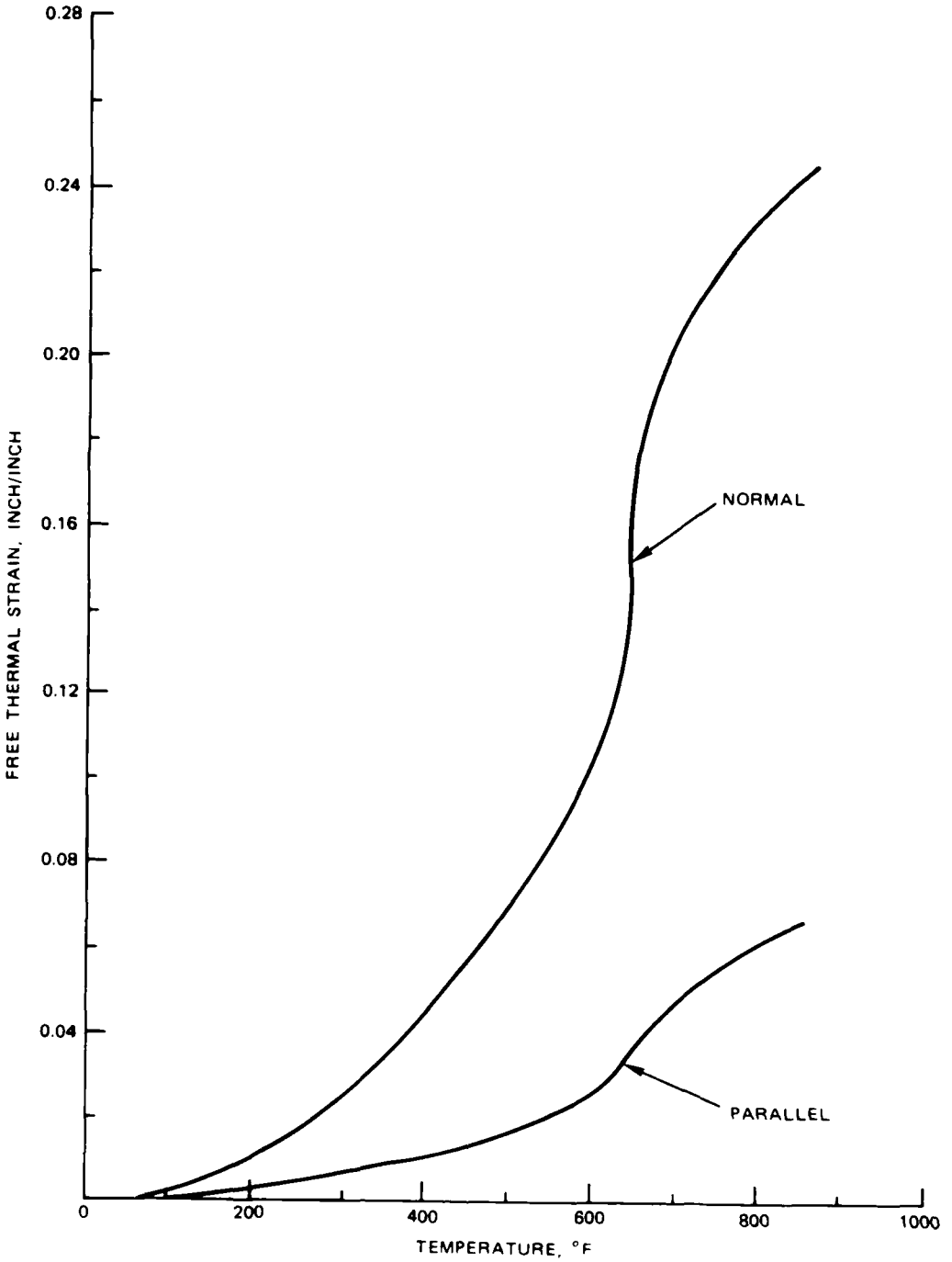

FIGURE 2-6. Thermal Expansion for Duroid 5870M.

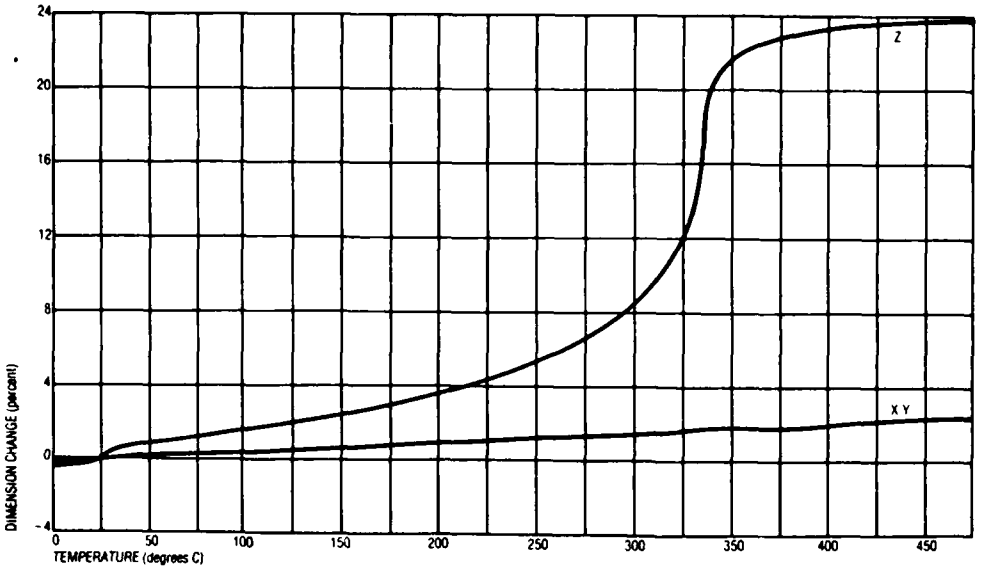

(a)

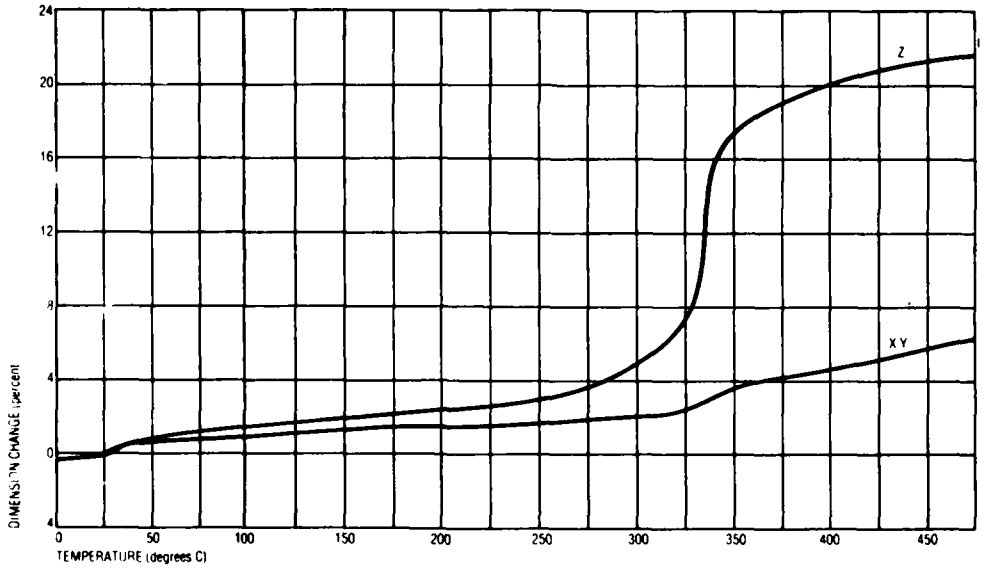

(b)

FIGURE 2-7. Thermal Expansion of RT/Duroid (a) 5870M and (b) 5650M.

are very similiar to those of Figure 2-6, they are not identical, even considering the different temperature scales.

Since the radome expands with increasing temperature, one could argue that the "effective" dielectric constant, which would be represented by the curve of increasing dielectric constant (with temperature) in Figure 2-5, is the quantity of most interest. Using this value, perhaps the radome could be treated as having a constant wall thickness but changing effective dielectric constant to a reasonable degree of approximation. In an actual missile flight, the radome will not come to some uniform temperature but rather will sustain temperature gradients that can be very substantial. On a low thermal conductivity material such as 5870M during a short missile flight, only a fairly thin outer layer may undergo a large change in temperature. The use of an "effective" dielectric constant while holding the radome dimensions constant with an "N-layer" analysis seems attractive, although its adequacy remains to be shown.

REFERENCES

2-1. R. E. Collin. Foundations for Microwave Engineering. New York, McGraw-Hill, 1966. P. 323.

2-2. -----. Field Theory of Guided Waves. New York, McGraw-Hill, 1966. Pp. 224-32.

2-3. -----. Foundations for Microwave Engineering. New York, McGraw-Hill, 1966. P. 315.

2-4. "High Frequency Dielectric Measurement," in Proceedings of a Tutorial Conference on Measurement of High Frequency Dielectric Properties of Materials, National Physical Laboratory, Teddington, U.K. 27-29 March 1972. J. Chamberlain and G. W. Chantry, eds. Place, PIC Science and Technology Press, Ltd., 1973. Pp. 12-13.

2-5. S. Ramo and J. R. Whinnery. Fields and Waves in Modern Radio. New York, John Wiley and Sons, 1953. Pp. 424-26.

3

MEASURING COMPLEX PERMEABILITY AND DIELECTRIC CONSTANT OF ISOTROPIC MATERIALS IN A COAXIAL TRANSMISSION LINE

A Hewlett-Packard (HP) 8410B automatic network analyzer is used to measure the complex reflection S11 and transmission S21 coefficients of a homogeneous sample that is placed in a 7-millimeter air line as shown in Figure 3-1. The air line connectors and air line are assumed to be lossless. The reflection coefficients S11 and S22 of the air line connectors are assumed to be zero. The line length from the measurement plane to the sample is the only parameter that is taken into account. This system allows measurements over a frequency range of 1 to 12.4 gigahertz. The frequency range is limited by the HP-8746 S-parameter test set being used in the current setup.

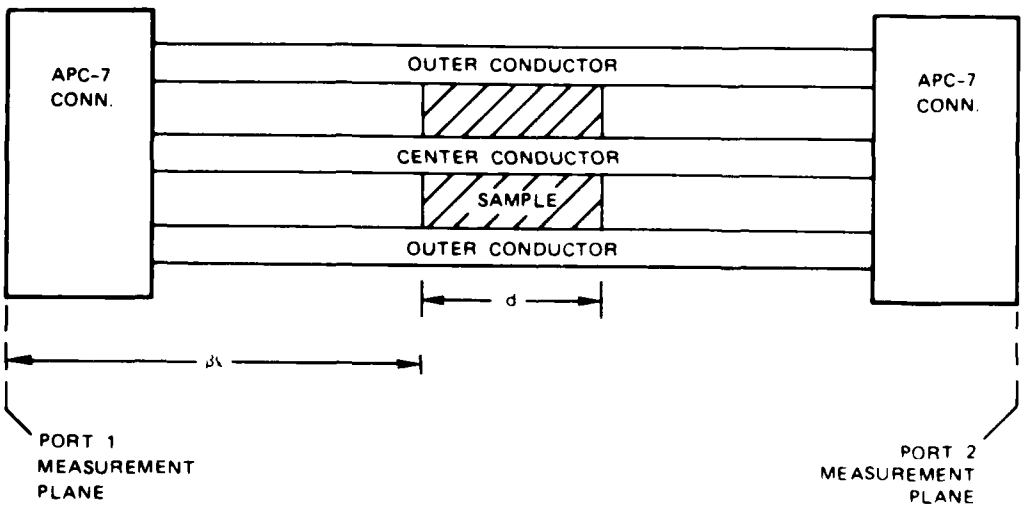

FIGURE 3-1. Cutaway View of Air Line With Sample.

The HP-8410B automated network analyzer system provides removal of the systematic errors caused by mismatch and leakage in the test setup, isolation between the reference and test channels, and the frequency tracking errors between test channels. These errors are removed by use of an 8-term error model (Reference 3-1). With this accuracy-enhancement software, the amplitude and phase of the scattering parameters can be measured to within 0.1 decibel and 1 degree, respectively. The sample holder is a 7-millimeter coaxial air line with APC-7 connectors. The sample is accurately positioned in the air line by means of a probe with a micrometer dial attached. S11abc and S21abc of the sample and sample holder, respectively, are measured, and S11b and S12b of the sample are given by Equations 3-1 and 3-2 below:

$$S11b = \frac{S11abc}{S21a\ S12a} \tag{3-1}$$

S11b is the reflection coefficient of the sample. S11abc is the measured reflection coefficient of the sample, air line, and its connectors (see Figure 3-2). S21a and S12a are the forward and reverse

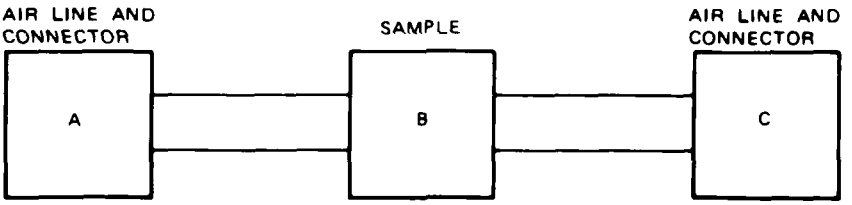

Connectors are assumed to be lossless with a reflection coefficient of zero. Air line is lossless.

FIGURE 3-2. Schematic of Air Line With Sample.

transmission coefficients, respectively, of connector a and the air line up to the sample interface, and they are given by

$$S12a = S21a = e^{-j\beta\ell_a}$$

where ℓ_a is the electrical line length from the Port 1 measurement plane to the sample interface and $\beta = 2\pi\nu/C$ (ν = frequency). The air line and its connectors are assumed to be lossless:

$$S12b = \frac{S21abc}{S12a\ S12c} \tag{3-2}$$

S12b and S21abc are the reverse transmission and the measured forward transmission coefficients, respectively, of the sample. S12a and S12c are the reverse transmission coefficient of the connectors a and c and the air line up to the sample interface.

$$S12c = e^{-j\beta\ell_c}$$

ℓ_c is the electrical line length from the sample interface to the Port 2 measurement plane.

Since we now have the complex reflection coefficient S11b and the complex transmission coefficient S12b of the sample, we can now compute the following complex equations that will give us the complex dielectric constant ε_c and complex permeability μ_c. The derivations of the following equations are presented in Reference 3-2.

$$V_1 = S11b + S12b \tag{3-3}$$

$$V_2 = S12b - S11b \tag{3-4}$$

$$X = \frac{(1 - V_1V_2)}{V_1 - V_2} \tag{3-5}$$

$$r = X \pm \sqrt{X^2 - 1} \tag{3-6}$$

Here r is the reflection at the boundary of the sample. Root r is chosen so that $|r| < 1$.

$$Z = \frac{V_1 - r}{1 - rV_1} \tag{3-7}$$

$$C_1 = \frac{(1 + r)^2}{(1 - r)^2} \tag{3-8}$$

$$C_2 = -\frac{C^2}{\omega^2} - d^2 \left(\ell n \frac{1}{|Z|} + j \arg \frac{1}{|Z|} \right)^2 \tag{3-9}$$

Here $\omega = 2\pi\nu$ and d is the thickness of the sample. The arg $1/Z = 2\pi n \cos^{-1} (Z'/|Z|)$, Z' is the real part of Z, and n is an integer that defines an ambiguity that occurs every 2π radians. From Equations 3-8 and 3-9, the complex dielectric constant is given by

$$\varepsilon = \sqrt{\frac{C_2}{C_1}} \tag{3-10}$$

$$\mu = \sqrt{C_1 C_2} \tag{3-11}$$

ERROR ANALYSIS

After measuring a few samples, including air, it became apparent that variations in the dielectric constant were systematic with frequency. These systematic errors were caused by a load mismatch and were not taken into account when calibrating the network analyzer (the 8-term error model does not include isolation and load-match errors). The 12-term error model requires that all four S-parameters be measured, but it provides for the best measurement accuracy of magnitude and phase. In the near future, the 12-term error model will be incorporated to determine if the dielectric constant accuracy can be improved over the technique that is presently being used.

To reduce measurement time, the present technique is to place a 10-decibel pad at the Port 2 measurement plane to reduce the voltage standing wave ratio (VSWR). The measured scattering parameters of an empty air line are then vectorially subtracted from the measurements performed with the sample in the air line. When measuring air with this technique, a dielectric constant of 1.000 is calculated with a standard deviation of 0.008. For Rexolite, the dielectric constant is 2.544 with a standard deviation of 0.047. Figures 3-3 and 3-4 are plots of these measurements.

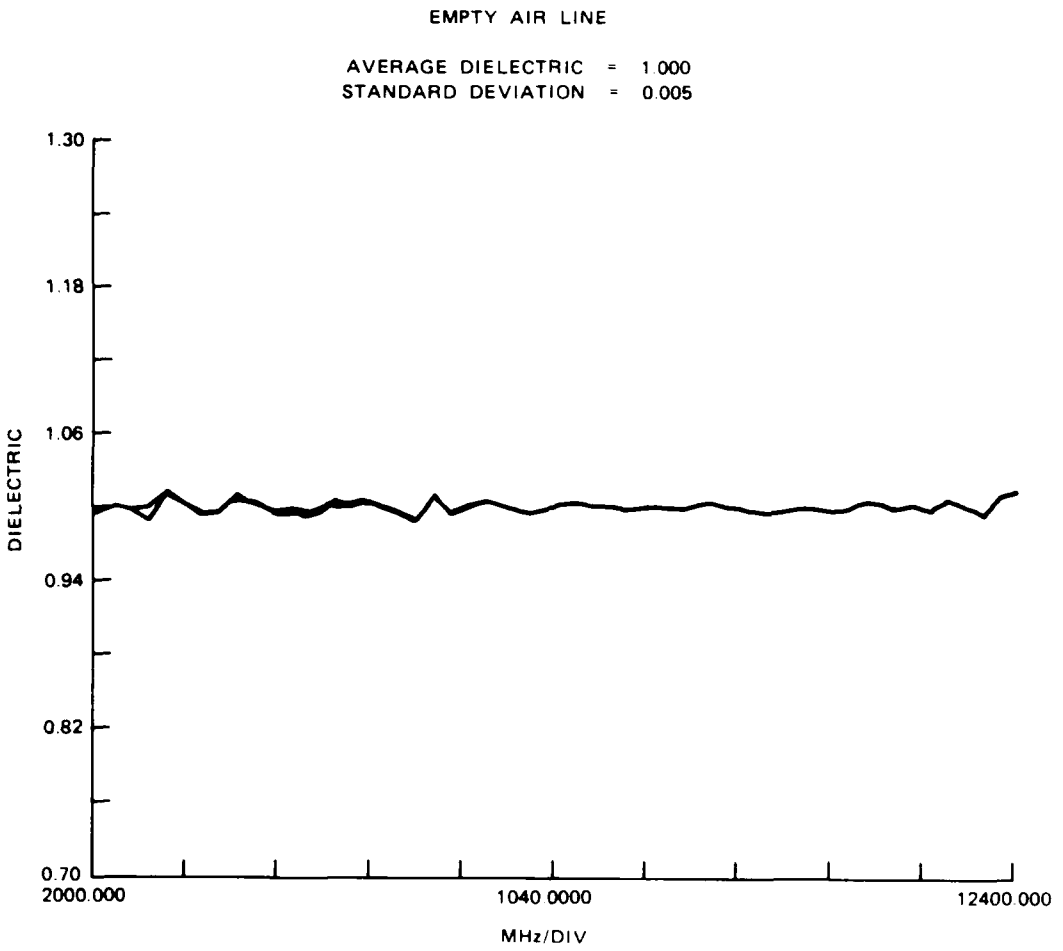

FIGURE 3-3. Measured Dielectric Constant of Air in the Empty Air Line.

To determine the effect of measurement errors S11 and S21 on the dielectric constant and permeability, known errors are imposed on calculated values of S11 and S12 and new values of dielectric constant and permeability are calculated. At this time, the errors study is just beginning. If the measurement system is the major source of error, then additional improvements can be made, such as employing a phase-locked radio frequency (RF) source to prevent harmonic skip. In this case, a different harmonic is selected by the network analyzer for the same test frequency between the time of calibration and measurement. Sample position error should be held to less than the 1-degree phase measurement error, which would be 2.6 mils at 12.6 gigahertz.

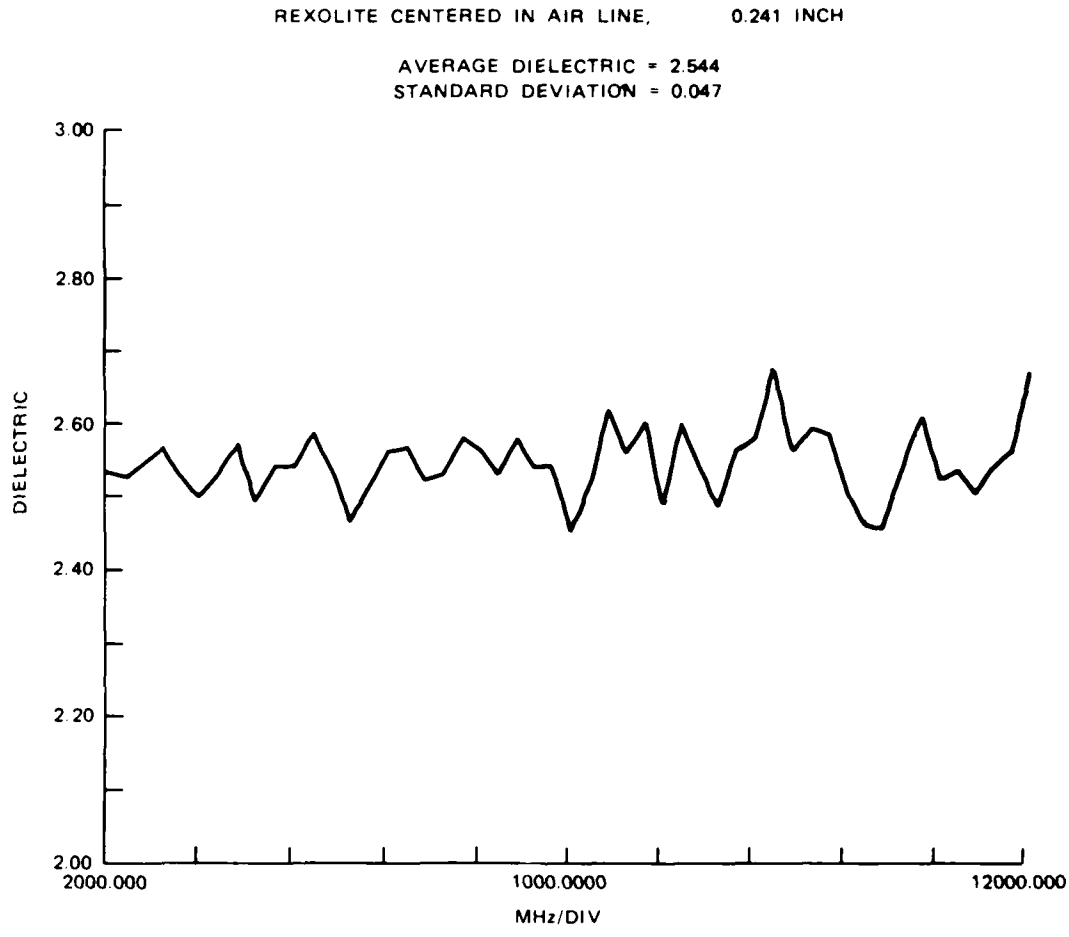

FIGURE 3-4. Measured Dielectric Constant of Rexolite in Coaxial Air Line.

Waveguide modes can propagate in high-dielectric or permeability materials. The cutoff frequency for the TE_{11} mode is given by

$$f_c = 0.293 \frac{V}{a}$$

where V is the velocity of light through the medium given by

$$V = \frac{C}{\sqrt{\varepsilon_r}}$$

C is the speed of light, and ε_r is the relative dielectric constant of the medium. Thus, for air the frequency at which a TE_{11} mode can propagate in a 7-millimeter air line is approximately 12.5 gigahertz. The waveguide mode can exist only in the sample itself, since the coaxial line will support only a transverse electromagnetic (TEM) wave at this frequency. Since the waveguide modes cannot be propagated in the air line, the energy is dissipated in the sample and makes the sample appear lossier than it really is. The strength of the waveguide mode is dependent upon the efficiency of the conversion of the TEM wave to a waveguide mode. This efficiency can be minimized by ensuring that the sample faces are perpendicular to the longitudinal axis of the sample and that the faces are smooth. Another source of error that needs to be investigated is the effect of a small air gap between the sample and the inner and outer conductors of the air line.

REFERENCES

3-1. "Automating the HP-8410B Microwave Network Analyzer," Hewlett-Packard Application Note 221A (June 1980).

3-2. A. M. Nicolson and G. F. Ross. "Measurement of the Intrinsic Properties of Materials by Time-Domain Techniques," IEEE Trans. Instrum. Meas., Vol. IM-19 (November 1970).

4

FREE-SPACE BRIDGE DIELECTOMETER

A free-space bridge is well suited for measuring the dielectric properties of materials at high temperature, since, ideally, the sample can be heated without producing effects caused by heating the measurement apparatus. In fact, the sample can be heated beyond the damage threshold, allowing destructive testing. The free-space bridge offers other advantages over cavity-type dielectric measurements. For instance, the free-space bridge is generally used with simple flat panel samples; whereas, for accurate results, closed-cavity measurements require machining the sample to very close tolerance. Also, the polarization and incidence angle of the impinging wave are widely variable in the free-space bridge. This is especially useful for studying anisotropic materials.

The free-space bridge does pose some specific disadvantages compared with a cavity dielectometer. While very precise measurements can be obtained in the free-space bridge dielectometer, its inherent accuracy is degraded by the inevitable presence of undesired reflections. The free-space measurement can track very small changes in the dielectric constant with change in temperature and can detect small differences between similar samples. However, for absolute accuracy, these difference measurements must be referenced to a measurement with better inherent accuracy, usually a resonant cavity-type measurement.

At NWC, a free-space bridge dielectometer has been constructed to measure the complex transmission coefficient of flat-panel samples at 35 gigahertz. The complex permittivity of the sample is calculated from the transmission measurements by iteration using a digital computer. An array of high-intensity heat lamps is used to heat the sample; bulk temperatures up to 1000°C have been obtained thus far.

A block diagram of the apparatus is given in Figure 4-1. The microwave beam is directed through the sample by a pair of lens-focused horns. For the current setup, the lens is focused to a 3-decibel-spot size of 1.5 wavelengths at an 18-inch focal distance. Because of spot-focusing the beam, samples only a few inches in diameter can be used without significant errors caused by diffraction at edges of the sample. The receive horn sits upon a carriage which moves the horn along and across the beam; micrometer screws read the position of the horn to

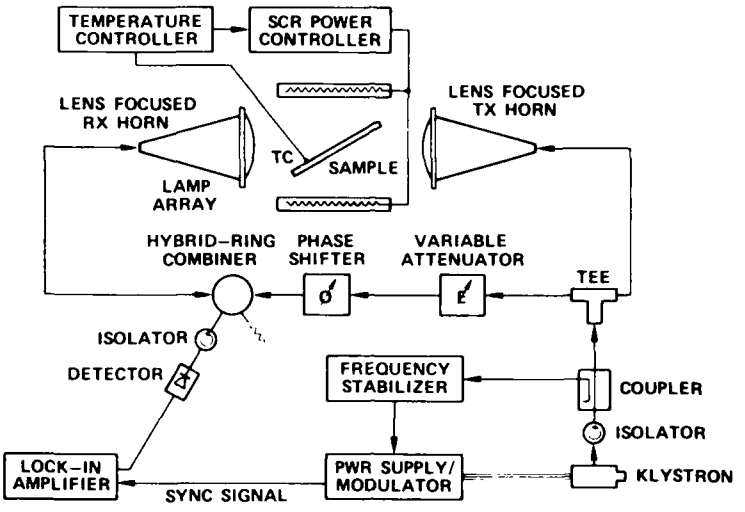

FIGURE 4-1. Block Diagram of the Free-Space Bridge Dielectometer.

0.0001 inch. The reference arm of the bridge contains a phase shifter and a variable attenuator that are used to precisely "null" and balance the bridge prior to inserting the test sample.

The signal from the free-space arm of the bridge is combined with the signal from the reference arm in a tuned hybrid. The combined signals reach a crystal detector producing a direct current voltage that depends on the relative phase and amplitude of the signals from the two bridge arms. A lock-in amplifier measures the detected signal voltage and provides greatly increased sensitivity over the use of a direct current voltmeter, permitting the measurement of a very small power imbalance on the bridge. This enhances the precision of the measurement and, in principle, allows the measurement of transmission loss through very low-loss materials.

The RF signal source is a 10-milliwatt klystron, operating at 35 gigahertz, that is phase-locked to a stable 5-megahertz quartz crystal oscillator. Without phase-locking the source, precision bridge measurements would be limited by frequency drift. The 35-gigahertz signal is square-wave modulated to provide a signal for the lock-in amplifier.

The sample heater consists of a set of ten high-intensity incandescent lamps with collimating parabolic reflectors. The lamps are arrayed in a circular arc on either side of the sample to focus their output onto a narrow strip on the sample surface. At full power, each

lamp produces an output heat flux of approximately 1 kilowatt on a 1.5- by 6-inch aperture with peak output at ~1-micron wavelength. The lamps are cooled by a recirculating water cooler.

The sample temperature is measured by a thermocouple placed below the surface of the sample. A programmable temperature controller, which is calibrated for the thermocouple, provides control of the bulk temperature of the sample. The controller senses the temperature of the sample and sends a signal voltage to a silicon-controlled rectifier (SCR) power controller that adjusts the lamp power to maintain a preset sample temperature or to change the temperature on a programmed time schedule.

Figure 4-2 is a photograph of the NWC free-space bridge dielectometer taken with the heat lamps turned on, producing the diffuse bright spot in the center of the picture. The transmit and receive horns are mounted on separate supports assembled from concrete blocks. The sample holder and heat lamp arrays are mounted together on a table that also supports the temperature/power controllers and a vent hood. The purpose of the vent hood is to draw away some of the waste heat produced by the lamps and to remove any gases that might be evolved by the hot sample. Also shown in Figure 4-2 is the rack that carries the electronic instrumentation for the dielectometer.

FIGURE 4-2. NWC Free-Space Bridge Dielectometer.

Initial calibration of the dielectometer is made by setting the phase shifter and attenuator in the bridge reference arm so that the bridge is precisely nulled and balanced, i.e., the output of the detector is zero without the sample in place. With the sample in place, the bridge is renulled at each temperature by adjusting the separation of the focused horns to obtain a minimum of the detected voltage. The phase shift through the sample is measured from the displacement of the micrometer, which moves the receive horn along the beam axis. This method of phase-shift measurement offers the best possible precision; it gives an accurately symmetrical interference minimum and restores the electrical distance between the horns to the same value as the initial calibration (plus some integer number of half-wavelengths).

Transmission loss through the sample is determined by measuring the power imbalance between the two bridge arms when the bridge has been adjusted to give a detected interference minimum with the sample in place. The power imbalance can be read directly from the variable attenuator in decibels of attenuation required in the reference arm to zero the detector output.

The magnitude of the sample voltage transmission coefficient can be determined from detector voltage readings without the need of detector calibration, provided that the detector exhibits proper square-law behavior over the dynamic range of the measurement. Using superposition of signals from the bridge reference and test arms for interference maximum and interference minimum, the magnitude t of the sample voltage transmission coefficient can be obtained in terms of detector output voltage levels. The quantity t is given by the following expression:

$$t = \frac{1 - \sqrt{P}}{1 + \sqrt{P}} \qquad (4\text{-}1)$$

where P is P_{max}/P_{min} -- the ratio of minimum to maximum detected power as the relative bridge phase is rotated 360 degrees with the sample in place. For a good square-law detector, P is the ratio of the maximum and minimum detector voltages.

Except in the case of normal incidence or for very thin samples, displacement of the microwave beam by refraction through the sample is important to the measurement of the transmission loss through the sample. For this reason, the receive horn can be moved laterally to the beam, using a micrometer screw to offset the deflection of the beam by

the sample. For a sample of thickness d and relative dielectric constant ε_r, the beam deflection as a function of incidence angle θ is given by

$$s = d \sin \theta \left[1 - \frac{\cos \theta}{\sqrt{\varepsilon_r - \sin^2 \theta}} \right] \tag{4-2}$$

Since the determination of the relative dielectric constant ε_r is nearly independent of the sample loss, it can be approximately measured without regard to beam deflection and then employed in the equation above for making a refined measurement.

Having measured the phase shift ΔL through the sample and the voltage transmission magnitude t, the relative dielectric constant and loss tangent of the test material are approximately given by the following expressions (Reference 4-1):

$$\varepsilon_r = 1 + 2 \frac{\Delta L}{d} \cos \theta + \left(\frac{\Delta L}{d} \right)^2 \tag{4-3}$$

$$\tan \delta = - \frac{\lambda \ell n(t) \sqrt{\varepsilon_r - \sin^2 \theta}}{\varepsilon_r \pi d} \tag{4-4}$$

Here λ is the free-space wavelength and θ is the plane-wave angle of incidence on the sample. These equations are valid for either linear polarization, but they are only approximate because they do not account for the effect of internal reflections at the sample surfaces. For the case in which the electric field polarization is parallel to the plane of incidence (parallel polarization), the error produced by use of these equations is generally smaller than for perpendicular polarization. In fact, for parallel polarization, the equations are exact at an angle of incidence equal to the Brewster angle,

$$\theta_B = \tan^{-1} \sqrt{\varepsilon_r} \tag{4-5}$$

in which case the interface reflection coefficient r_i is equal to zero. For either polarization, the maximum measurement error of ΔL is equal to (Reference 4-2)

$$\frac{\lambda}{2\pi} \sin^{-1} (r_i)^2 \tag{4-6}$$

For arbitrary polarization and angle of incidence, the interface reflection from the sample cannot be ignored and the generalized flat-panel transmission coefficient must be employed. The complex transmission coefficient for a plane wave incident on a flat sample in air can be obtained by satisfying boundary conditions and using Snell's law at both sample surfaces for incident, reflected, and transmitted waves (Reference 4-3). The transmission coefficient thus obtained for non-magnetic materials ($\mu = \mu_o$) is given by

$$T_i = \frac{(1 - r_i^2)\exp -j\beta_o d(\cos\theta + \sqrt{\varepsilon_r - \sin^2\theta})}{1 - r_i^2 \exp(-2j\beta_o d\sqrt{\varepsilon_r - \sin^2\theta})} \tag{4-7}$$

where d is the sheet thickness and θ is the angle of incidence; β_o is the free-space wave number equal to $2\pi/\lambda_o$. The relative dielectric constant of the sample sheet is ε_r. For lossy material, this is replaced by the complex relative dielectric constant, $\varepsilon_r(1 - j \tan\delta)$, in which $\tan\delta$ is the so-called loss tangent or dissipation factor of the material. The interface reflection coefficient or Fresnel coefficient r_i depends on the polarization of the incident wave. For electric field parallel to the plane of incidence requiring tangential E and H fields to be continuous across the interface gives the following formula for interface reflection coefficient (Reference 4-4):

$$r = \frac{\varepsilon_r \cos\theta - \sqrt{\varepsilon_r - \sin^2\theta}}{\varepsilon_r \cos\theta + \sqrt{\varepsilon_r - \sin^2\theta}} \tag{4-8}$$

For electric field polarized perpendicular to the plane of incidence, the same boundary conditions will stipulate the following relation for r_i:

$$r = \frac{\cos\theta - \sqrt{\varepsilon_r - \sin^2\theta}}{\cos\theta + \sqrt{\varepsilon_r - \sin^2\theta}} \tag{4-9}$$

Once again, for the validity of these equations, we have assumed that the material is nonmagnetic and surrounded by air or vacuum.

By the measurement procedures previously described, we obtain the magnitude and phase of the complex transmission coefficient, given by Equation 4-7, for the sample being tested. With all of the other measurement parameters known, the equation can, in principle, be solved for the complex dielectric constant of the sample. Lacking a formula that expresses the dielectric constant in terms of the measurement parameters, Equation 4-7 must be solved by numerical techniques using a digital computer.

The numerical approach proceeds as follows. Using an initial estimate for the dielectric constant, a test value for the complex transmission coefficient is calculated from Equation 4-7. The test value is subtracted from the measured value of the transmission coefficient to define a test function of the dielectric constant. The root of the test function, which we obtain using an algorithm based on Muller's method (Reference 4-5), is the desired complex dielectric constant of the material. The computer program, which is run on an HP-1000 computer, appears in Appendix A.

Actually, there is an infinite number of dielectric constant values which will solve Equation 4-7 for a given value of T. This does not present a problem if the initial estimate is reasonably close to the actual value. For a totally unknown sample, a very good initial estimate can be obtained by finding the angle of incidence that gives maximum transmission through the sample for parallel polarization. This being the Brewster angle, the relative dielectric constant is obtained from Equation 4-5, although the precision is limited by the precision of the angle measurement.

Dielectric constant data have been obtained for a few sample materials at room temperature, and the results are presented in Table 4-1. These are primarily electromagnetic window materials that have been provided by industry. The data were taken over a range of incidence angles, and the relative dielectric constant given in the table represents an average of the data for each sample, assuming the materials are basically isotropic. The uncertainty that is given is equal to one standard deviation for the data set. Table 4-2 gives reference data provided by the manufacturer or reported by independent investigators.

TABLE 4-1. Room Temperature Data.

Manufacturer	Material	ε_r
Rogers Corp.	Duroid 5880	---
Rogers Corp.	Duroid 5870	2.41 ± 0.02
Omohundro Corp.	1-Cerez	1.98 ± 0.02
Omohundro Corp.	1-Cerez	1.93 ± 0.03
Corning Glass Works	Pyroceram 9606	5.64 ± 0.04
Dynasil Corp.	Dynasil 4000 (fused quartz)	3.77 ± 0.05

TABLE 4-2. Dielectric Reference Data.

Source	Material	ε_r	tan δ
Manufacturer	Duroid 5880[a]	2.20 ± 0.02	0.0009
Manufacturer	Duroid 5870[a]	2.33 ± 0.02	0.0012
Manufacturer	1-Cerez	1.95 - 2.15	0.017
Manufacturer	2-Cerez	1.65	0.003
Reference 4-5	Pyroceram 9606	5.57	0.0003
Reference 4-6	Dynasil 4000 (fused quartz)	3.82	0.0003

[a]Data taken at 10 gigahertz.

Loss tangent measurements for these low-loss materials were found to vary widely with incidence angle because of systematic effects; thus, the results are not reported here. While the accuracy was poor, the sensitivity obtained for loss tangent measurements using this apparatus is quite good. Changes in transmitted power through the sample can easily be resolved to 0.01 decibel, making the apparatus very useful for measuring changes in the value of the sample loss tangent as it is heated. For absolute accuracy, measured changes can be referenced to baseline data obtained at room temperature with a more accurate cavity-type measurement, such as the open resonator measurements described in the following section.

High-temperature measurements of the relative dielectric constant have been obtained for fused quartz up to a temperature of 900°F. Higher temperatures could be obtained by blackening the surface of the sample since quartz is nearly transparent at the peak output wavelength of the heat lamps. Figure 4-3 shows a plot of the measured results along with measurements made by W. Ho of Rockwell Science Center

(Reference 4-7). Ho claims a measurement accuracy of better than 1%, and our results agree with his to within about 2%.

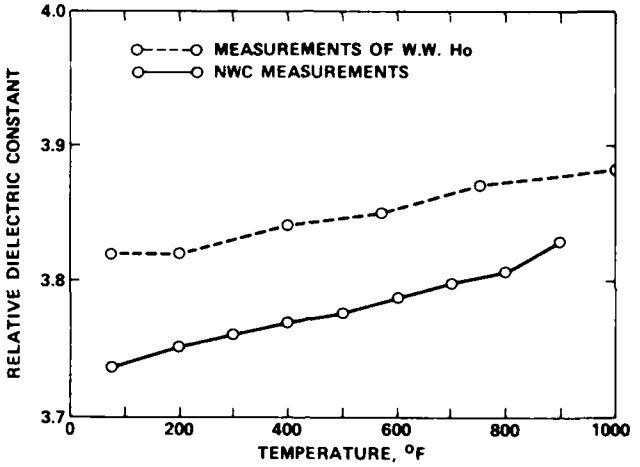

FIGURE 4-3. High-Temperature Measurements of Fused Quartz Sample.

To obtain the best possible sensitivity and accuracy with the apparatus, a number of possible sources of error must be considered:

Mechanical backlash in the receive-horn positioner
Instrument drift over time
Sample thickness variability
Sidelobes and diffraction at sample edges
Thermal effects due to indirect heating of the apparatus
Presence of standing waves

The mechanical backlash problem occurs when the direction is reversed while adjusting the positioner to null the bridge. The error can be as large as 0.001 inch in air but can be eliminated almost entirely by making the final adjustment in the forward direction. After an initial 2-hour warm-up, instrument drift is insignificant if the measurement is carried out within 10 minutes or so of initial calibration. For best accuracy, the sample should have uniform thickness to at least the desired precision of the measurement. However, since the measurement is actually an average over the surface of a spot illuminated by the Gaussian beam, an appropriate average value taken

for the sample thickness should give satisfactory results. While antenna sidelobes are certainly present, they produce no measurable effect in the apparatus unless they are scattered by obstacles placed in certain "hot spots" near the antennas. We have found that diffraction at the edges of the sample is insignificant if the sample presents a cross section of as little as 3 inches across the microwave beam. Indirect heating of the antenna focusing lenses can produce large errors in a short time if thermal isolation is not provided while the sample is being heated. This problem is solved by placing a shield of refractory material in front of each lens while the heat lamps are on and briefly turning off the lamps while a measurement is being made.

Although there are isolators ahead of the detector and in each arm of the bridge, there is a standing-wave ratio on the order of 1.2:1 between the two focused horns. Additional reflections anywhere on the bridge will produce error dependent on the electrical separation of the reflections. At this point, it is impractical to try to further reduce the reflections in the system, but it may be possible to quantify the effects of the standing waves, using an appropriate model for the system, and subsequently subtract these effects from the measurement. A model has been developed that may prove useful for enhancing the accuracy of the free-space dielectometer. A graphical exposition of the model is presented in Appendix B.

At the present time, the most basic limitation to the accuracy of measurements in the lens-focused, free-space bridge is the result of the Gaussian character of the wave front that is incident on the sample. The dielectric constant is calculated from the measured transmission coefficient according to Equation 4-7, which is actually derived for the case of an incident plane wave. Since the phase and amplitude are complicated functions of position in the incident beam, Equation 4-7 gives only an approximate description of transmission through the sample, and the errors produced increase with higher dielectric constant. At this point, it is unclear whether it may be practical or possible to formulate a model that accurately accounts for the Gaussian character of the beam in this type of measurement. If it can be done, this would be a significant accomplishment because of the inherent precision, ease, and flexibility of the free-space bridge measurement.

Other work to be undertaken in the near future includes the addition of a reflection-measurement capability to this apparatus. By measuring complex reflection and transmission coefficients of a sample, the permeability and permittivity of the sample can both be obtained. The reflection measurement capability would also be useful for the study of microwave and millimeter-wave absorbing materials.

Since the lens-focused horn antennas used in this apparatus are essentially frequency independent, the apparatus could be used in other

frequency ranges by the addition of the appropriate waveguide "plumbing." Current plans include testing the apparatus in Ku band.

The apparatus could be partly automated using a readily available, high-precision linear positioner under computer control. By providing a digital output for the detector voltage to the computer, the data could be acquired automatically by the use of a null-seeking algorithm to position the receive horn. This approach could greatly increase the accuracy of the data by eliminating mechanical backlash error and by minimizing sample temperature drift in a much faster measurement cycle. The effort to partially automate the free-space bridge dielectometer is in progress at the present time.

REFERENCES

4-1. R. M. Redheffer. "The Measurement of Dielectric Constants," in Technique of Microwave Measurements, C. G. Montgomery, ed. New York, McGraw-Hill, 1947. Pp. 600-602.

4-2. ------. P. 601.

4-3. Techniques for Airborne Radome Design. Dr. T. E. Tice, ed. New York, McGraw-Hill, 1966. Vol. 1, pp. 31-32.

4-4. J. D. Jackson. Classical Electrodynamics, 2nd ed. New York, John Wiley & Sons, Inc., 1975. Pp. 280-281.

4-5. Massachusetts Institute of Technology. Tables of Dielectric Materials, Volume VI, by W. B. Westphal. Cambridge, Mass., MIT, Laboratory for Insulation Research, 1958, p. 42. (MIT Technical Report 126, publication UNCLASSIFIED.)

4-6. ------. Dielectric Measurements on High Temperature Materials, by W. B. Westphal and J. Iglesias. Cambridge, Mass., MIT, Laboratory for Insulation Research, 1970, p. 39. (Technical Report AFML-TR-70-138, report UNCLASSIFIED.)

4-7. Army Materials and Mechanics Research Center. High Temperature Millimeter Wave Characterization of the Dielectric Properties of Advanced Window Materials, by W. W. Ho. Watertown, Mass., AMMRC, 1982. (Technical Report AMMRC-TR-83-28, report UNCLASSIFIED.)

5

FABRY-PEROT RESONATOR FOR DIELECTRIC MEASUREMENTS

The Fabry-Perot-type resonator is very useful for measuring dielectric properties of materials and offers a high degree of accuracy and relative ease of use. The measurements can be made with the same flat panel samples used in the free-space bridge dielectometer, making the resonator useful for providing accurate room-temperature reference data for the high-temperature measurements described in the previous section.

The resonator is configured as a semiconfocal resonator: one plane mirror and one spherical mirror. This configuration is less sensitive to a slight misalignment of the two mirrors than for the case with two plane mirrors. Both mirrors are machined from brass. There is a single iris in the center of the plane mirror to couple into the resonator. The spherical mirror can be moved along the symmetry axis of the resonator using a precision micrometer drive that reads out to 0.001 millimeter. Figure 5-1 is a schematic diagram of the resonator showing dimensions that pertain to the measurement of dielectric constant. Referring to the diagram R_o, the radius of curvature of the spherical mirror is 5.00 inches. L is the length of the cavity at resonance for a particular mode without the sample in place. ΔL is the mirror displacement required to restore resonance at the same mode after the sample is placed in the resonator.

With the sample placed against the flat mirror, as shown in Figure 5-1, the relative dielectric constant ε_r is obtained from the index of refraction, which is given by (Reference 5-1)

$$\frac{\tan(n\beta d)}{n\beta d} = \pm \frac{\tan \beta(d + \Delta L)}{\beta d} \qquad (5\text{-}1)$$

where $n = \sqrt{\varepsilon_r}$ and $\beta = 2\pi/\lambda_o$. The equation is solved for n by numerical iteration.

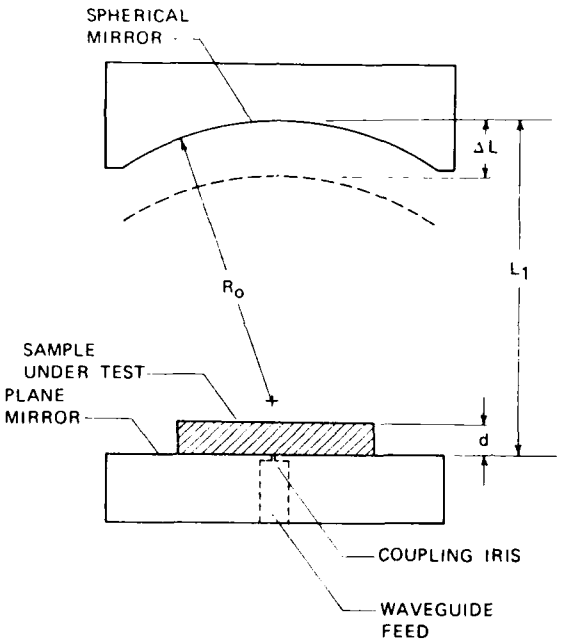

FIGURE 5-1. Schematic Diagram of the Semiconfocal Resonator.

The loss tangent of a sample is determined by measuring the quality factor Q_o of the empty resonator and Q of the resonator with the sample in place. Quite generally, the Q of a cavity depends on the strength of the coupling into the cavity. The Q of a cavity is defined as

$$Q = \frac{\text{energy stored}}{\text{energy lost}} \text{ per cycle}$$

As the coupling is increased, the oscillation in the cavity is more rapidly damped and therefore Q is decreased. Placing the test sample directly against the coupling iris in the flat mirror, as shown in Figure 5-1, changes the coupling of the resonator. Since we are interested in measuring the change in Q of the resonator, which is produced solely by loss in the sample, the sample must be spaced some distance away from the flat mirror to avoid affecting the coupling. At 35 gigahertz we have obtained adequate results with spacing as little as 0.065 inch off of the flat mirror.

The Q of the cavity can be measured by noting the width between half-power points on the resonance line as the micrometer is turned and using

$$Q = \frac{L}{\Delta L}$$

where L is the length of the cavity and ΔL is the 3-decibel displacement. ΔL can be measured with precision up to four significant digits. Much more accurate is the frequency change method where Q is given by

$$Q = \frac{f_o}{\Delta f}$$

The 3-decibel linewidth Δf can be read with precision up to nine significant digits, depending on the stability of the RF source.

The loss tangent of a sample is measured by the following procedures:

- Obtain resonance in the empty resonator by moving the spherical mirror and note the length L_1 of the cavity at resonance.
- Measure Q_o of the empty resonator by frequency change.
- Insert sample into the resonator using spacers to space the sample away from and parallel to the plane mirror.
- Return resonator to resonance at the same TEM_{ooq} mode obtained in the empty cavity by reducing the length of the cavity using the micrometer.
- Measure Q of the cavity with the sample by frequency change.

For samples of thickness greater than $\lambda/2$, the loss tangent is given approximately by the following expression (Reference 5-2):

$$\tan \delta = \frac{Z_1/Q - L_1/Q_o}{(A_1/A_o)^2 E_r d + 1} \qquad (5\text{-}2)$$

where

$$Z_1 = L_1 - d - \Delta L \tag{5-3}$$

and

$$\left(\frac{A_1}{A_o}\right)^2 = \frac{1 + \cot^2 (n\beta d)}{1 + n^2 \cot^2 (n\beta d)} \tag{5-4}$$

If $d = \lambda/2$, the error in Equation 5-2 is approximately 10%, which is comparable to the typical experimental error at these wavelengths.

Equation 5-2 is derived by volume integrations of the energy density in the resonator, so (to the extent that curvature of the wave front incident on the sample can be ignored) the spacing of the sample from the plane mirror is unimportant. In actuality, plane waves exist only at the surface of the plane mirror; thus, for a sample of appreciable thickness or large separation from the plane mirror, Equations 5-1 and 5-2 must be corrected for wave-front curvature. A number of different approaches to calculating the corrections have been worked out including the methods of Cullen and Yu (Reference 5-3), Cook and Jones (Reference 5-4), and Lynch (Reference 5-5). At the present time, these corrections are smaller than the typical measurement errors that are encountered using the NWC apparatus; thus, for the data herein reported, these corrections are not employed.

Figure 5-2 shows a block diagram of the NWC laboratory setup for dielectric measurements using the Fabry-Perot resonator. The RF source consists of a microwave sweeper that is phase-locked to the internal time base of a phase-locking frequency counter (EIP Model 578). This arrangement can be used much like a microwave/millimeter wave synthesizer, since the output frequency of the sweeper can be controlled by front panel numerical input to the frequency counter with a resolution of 10 kilohertz. Directional couplers are used to sample equally the power incident on and power reflected from the resonator coupling iris at the end of the waveguide feed. Matched crystal detectors are used to measure the ratio of reflected/incident power that is displayed on a scalar network analyzer. By ratioing the reflected and incident power levels, measurements are made less sensitive to amplitude fluctuations or amplitude modulation noise from the sweeper.

The resonator itself is constructed to accept interchangeable feeds to cover multiple frequency bands, currently at 26.5 to 40 gigahertz and 60 to 90 gigahertz. At 35 gigahertz, the resonator exhibits a maximum loaded Q of 20 000. At the present time, no measurements

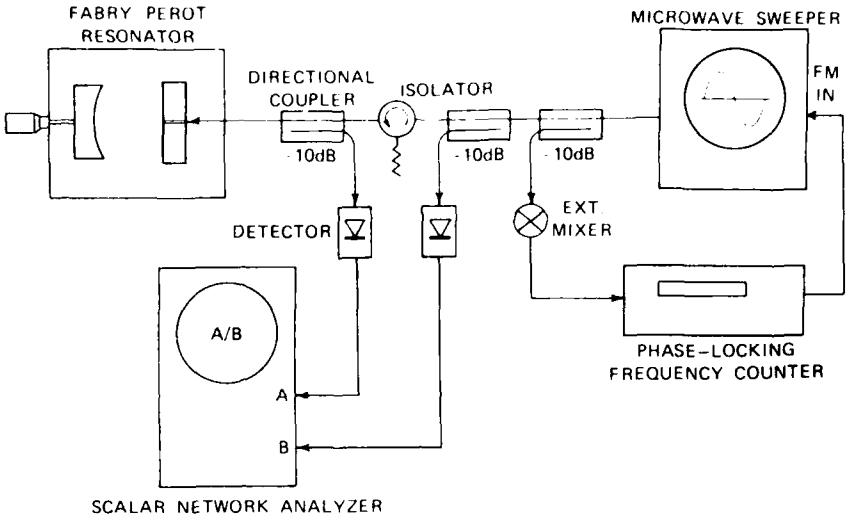

FIGURE 5-2. Block Diagram of Setup for Dielectric Measurements.

have been made in the higher frequency band. Figure 5-3 is a photograph of the resonator with a dielectric sample in place and spacers used for loss measurements. Figure 5-4 shows the interchangeable waveguide feeds that are used with the resonator.

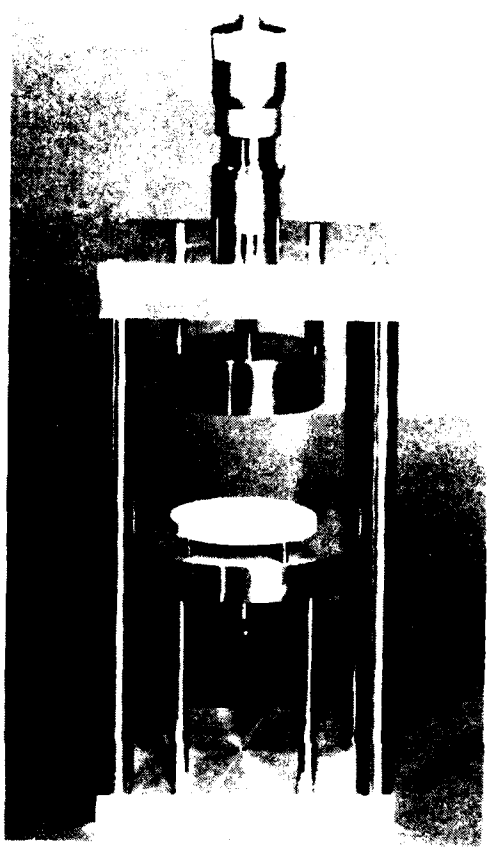

FIGURE 5-3. The Fabry-Perot Resonator With Dielectric Sample in Place.

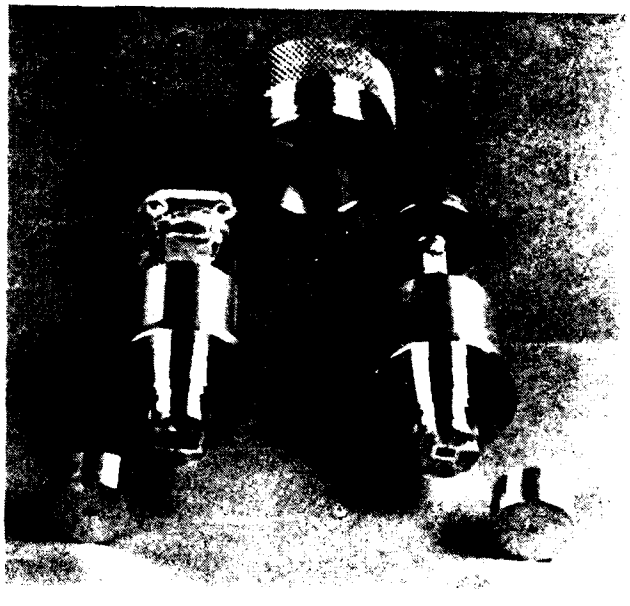

FIGURE 5-4. Interchangeable Ka-Band and E-Band Feeds for the Fabry-Perot Resonator.

Measurements of dielectric constant and loss tangent were made at 35 gigahertz in the Fabry-Perot resonator for comparison with data obtained in the free-space bridge dielectometer (Table 5-1). The results from the resonator measurements are presented in the table.

TABLE 5-1. Resonator Measurements.

Material	ε_r	tan δ
Duroid 5880	----	----
Duroid 5870	2.22	0.0012
1-Cerez	1.98	0.0056
2-Cerez	1.94	0.0021
Pyroceram 9606	5.63	0.00026

At present, the sensitivity of the measurements made in the Fabry-Perot resonator apparatus is limited by the stability of the RF source. By employing a phase-lock loop with wider loop bandwidth and a more stable reference, the RF frequency could be controlled to a resolution of 100 hertz or better. Addition of an automatic gain control for the RF source could also enhance the measurement precision. Synchronous-detection and/or signal-averaging techniques would allow the possibility of looser coupling to the cavity, thereby increasing the Q factor. Much work remains to be done in terms of acquiring data on materials in the 35-gigahertz range and above. This effort shall proceed as more materials become available for testing.

REFERENCES

5-1. K. H. Breeden and J. B. Langley. "Fabry-Perot Cavity for Dielectric Measurements," Rev. Sci. Instrum., Vol. 40, No. 9 (September 1969), p. 1162.

5-2. ------. P. 1163.

5-3. A. L. Cullen and P. K. Yu. "The Accurate Measurement of Permittivity by Means of an Open Resonator," Proc. R. Soc. London, Ser. A, Vol. 325 (1971), pp. 493-509.

5-4. R. J. Cook and R. G. Jones. "Correction to Open-Resonator Permittivity or Loss Measurements," Electron. Lett., Vol. 12 (1976), pp. 1-2.

5-5. A. C. Lynch. "Measurement of Permittivity Using an Open Resonator," IEE Proc., Vol. 130, Pt. A, No. 7 (November 1983), pp. 365-68.

6

COMPUTER-CONTROLLED MOVING VANE DIELECTRIC CONSTANT MEASUREMENT SYSTEM

The complex propagation constant γ and characteristic wave impedance Z of a material are determined by the complex relative dielectric permittivity $\varepsilon^* = \varepsilon(1-j \tan \delta_e)$ and magnetic permeability $\mu^* = \mu(1-j \tan \delta_m)$. For free-space propagation, the relations are

$$\gamma = \gamma_o \sqrt{\mu^* \varepsilon^*} \tag{6-1a}$$

$$Z = Z_o \sqrt{\frac{\mu^*}{\varepsilon^*}} \tag{6-1b}$$

For a material of thickness ℓ backed by a conducting surface, the complex reflection coefficient $\Gamma(\ell)$ is given by

$$\Gamma(\ell) = \frac{\Gamma(\infty) - e^{-2\gamma\ell}}{1 - \Gamma(\infty)^{-2\gamma\ell}} \tag{6-2a}$$

where

$$\Gamma(\infty) = \frac{Z - Z_o}{Z + Z_o} \tag{6-2b}$$

The quantity $\Gamma(\infty)$ represents the limit $\gamma\ell \gg 1$ and corresponds to the empty space/material interface reflection coefficient. In guided-wave structures, the parameters γ and Z are determined by ε^* and μ^* as well as the frequency and waveguide dimensions (see Appendix B).

The moving vane dielectometer is illustrated in Figures 6-1(a) and (b). The moving vane is a solid metal bar that completely fills the waveguide. A slot is cut in this bar to accommodate the sample to be measured. The width of this slot is made sufficiently small such that it represents a waveguide well below cutoff when loaded with the dielectric sample. The sample is centered in the waveguide and remains stationary during a measurement. The vane is driven by a stepper-motor assembly. Figure 6-1(b) illustrates three positions of the vane relative to the sample. For the upper drawing (sample recessed), the vane approximates a moving short. In the lower drawing, the vane is recessed and the sample inhomogeneously fills the waveguide. The "effective" sample length is determined by the vane position and is varied continuously during a measurement. A detailed analysis of the inhomogeneously filled waveguide is presented in Appendix C.

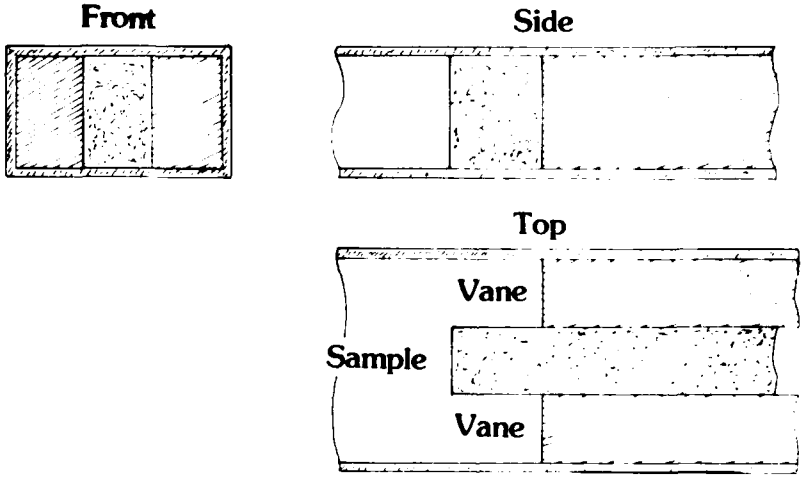

(a)

FIGURE 6-1. Sample and Moving Vane Assembly.

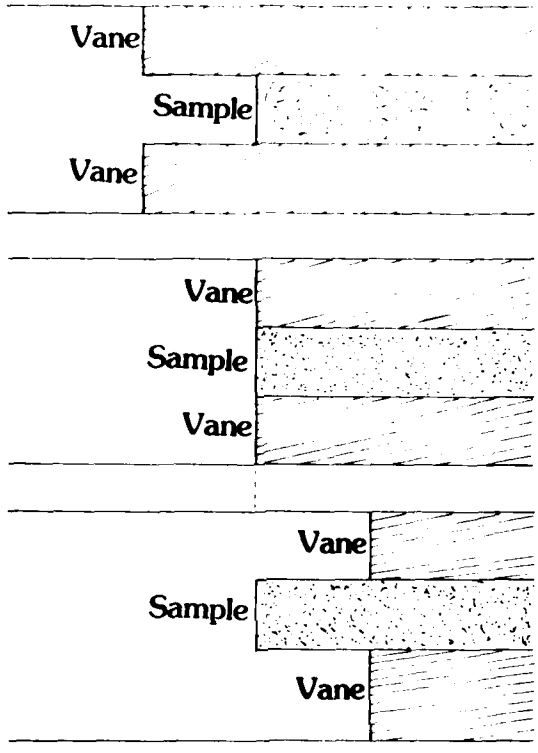

(b)

FIGURE 6-1. Contd.

A block diagram of the measurement system is shown in Figure 6-2. Measurement errors arise from the non-square-law power dependence of the mixer crystals (see Appendix D) and their power-level-dependent direct current offsets. The former is eliminated by inserting 20- to 30-decibel attenuation (step attenuator) in the signal arm. To eliminate direct current offsets, four independent measurements are made versus sample position at the relative phases (precision phase shifts) 0, 90, 180, and 270 degrees. Subtracting data pairs (0 to 180 degrees and 90 to 270 degrees) provides the corrected in-phase and quadrature components of the reflection coefficient. This procedure is performed for each vane position in a measurement set.

The moving vane system has been automated and is controlled by an HP-1000/F computer. A special digital interface has been designed that controls stepper-motor acceleration, synchronizes stepper-motor position and data acquisition, and repositions the vane to precise initial positions. For each of the reference phase values, the vane is cycled

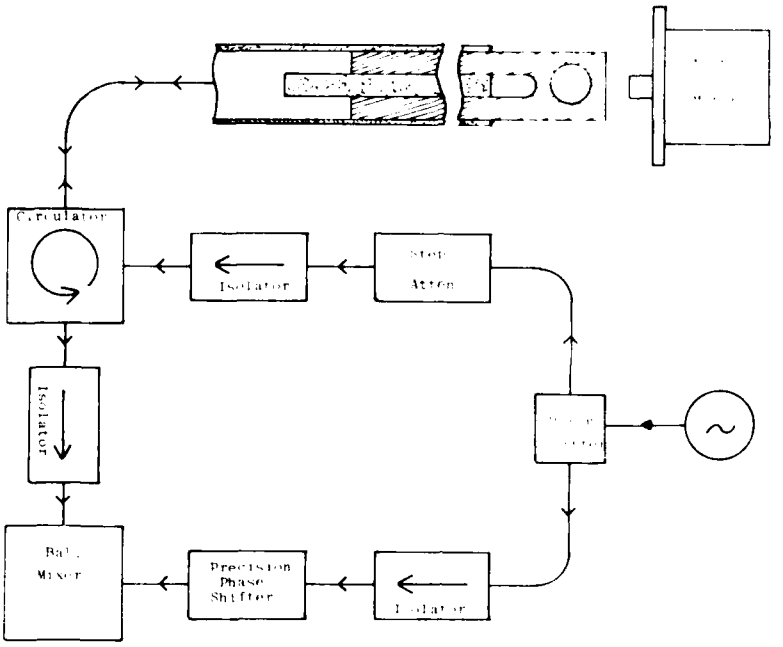

FIGURE 6-2. Block Diagram of the Moving Vane Dielectric Measurement System.

from minimum to maximum to minimum vane insertion positions. Data for each cycle are stored as a disk file and the subtractions are performed with software. The total sample measurement time is under 4 minutes.

A series of measurements on different representative materials has been performed. The measurement conditions were F = 9.7 gigahertz and sample (slot) widths of 0.2 inch in rectangular X-band waveguide. Results for a 6-guide-wavelength-long Teflon sample gives ε = 1.966. Individual half-wavelength segments were analyzed and averaged over the sample length giving a root-mean-square deviation of 0.64%.

Data for a Bakelite sample were obtained and are plotted as sin(phase) and phase versus position in Figures 6-3(a) and (b), respectively. The "empty" and "inhomogeneously filled" regions of relative vane position are readily apparent from the period differences. The distortion in the "filled" region is caused by the standing wave established between the empty/filled waveguide interface and the vane position. The standing wave contribution is illustrated in Figure 6-3(b) for phase versus position. In the absence of the interface/vane standing wave contributions, the empty/filled regions would have constant

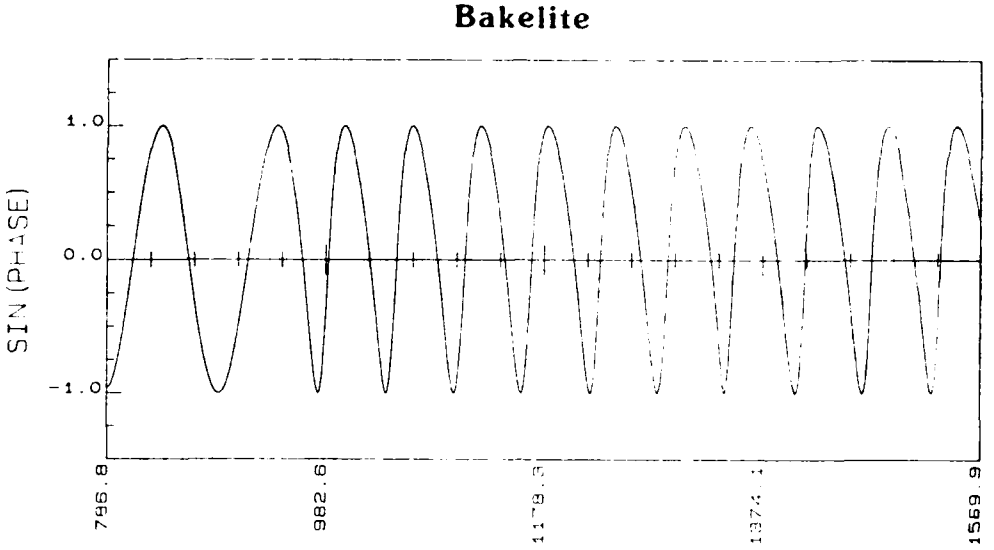

(a)

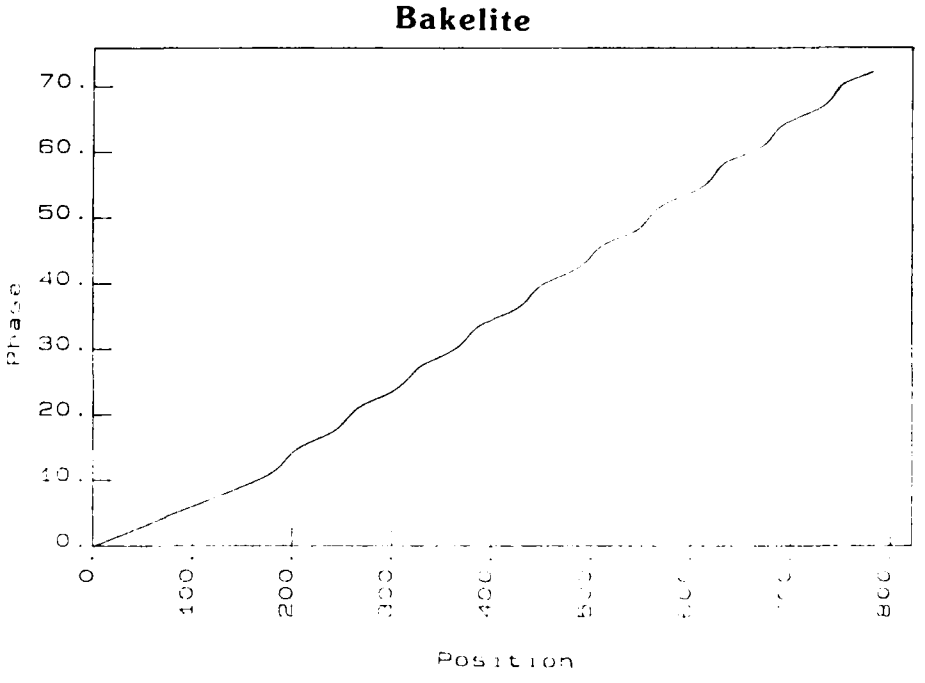

(b)

FIGURE 6-3. Measured Data for Bakelite.

slopes inversely proportional to the guide wavelength. The result for this sample is $\varepsilon = 3.054$. The root-mean-square standard deviation of 2.2% compared to the result of 0.6% for Teflon indicates the inhomogeneity of the dielectric constant.

Figure 6-4 is the sin(phase)-versus-position variation for a metal foam artificial dielectric microwave lens material. A close inspection of this figure indicates substantial volume inhomogeneity in the dielectric constant. The average value, $\varepsilon = 2.96$, exhibits a root-mean-square deviation of 3.8% from the mean.

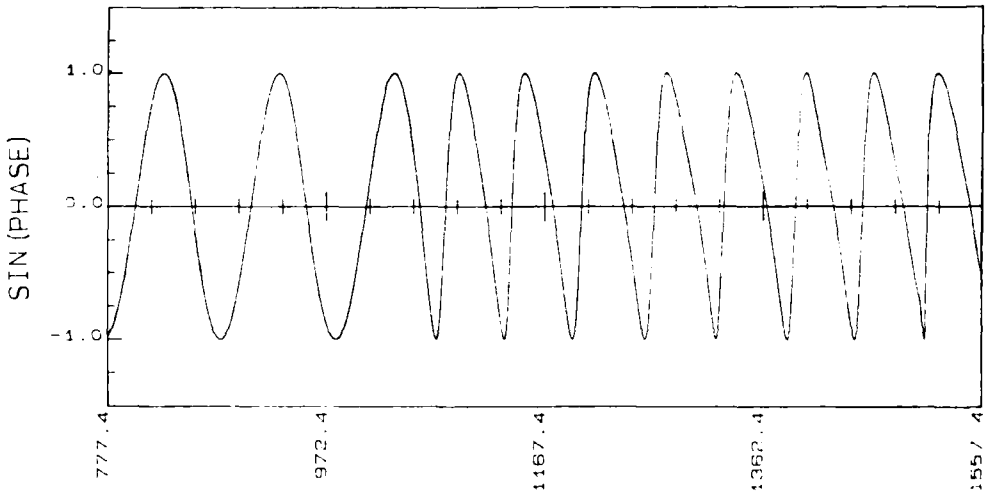

FIGURE 6-4. Sin(Phase) Variation for Metal Foam Artificial Dielectric.

Figures 6-5(a) and (b) are initial results for a special composite magnetic absorber. The results in Figure 6-5(a) show the magnitude of the reflection coefficient versus sample length for a rectangular sample. The results in Figure 6-5(b) show the same material tapered from zero to full height over a length of approximately 3 guide wavelengths. Effective elimination of the interface reflection will facilitate determination of absorption coefficients in this class of highly absorbing materials.

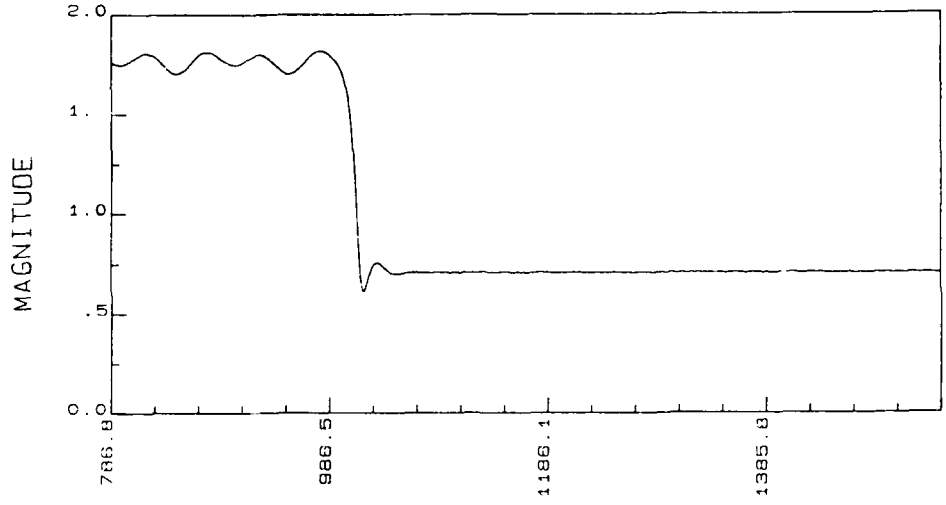

(a)

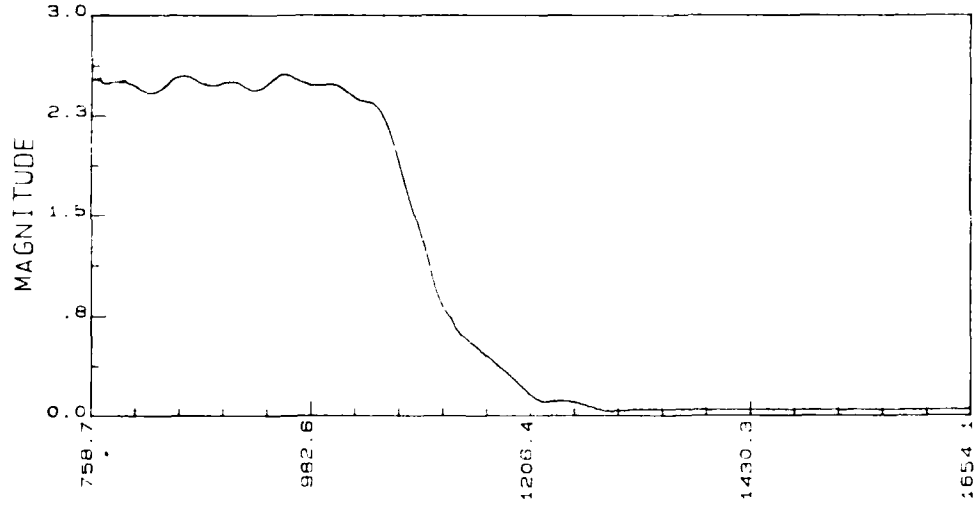

(b)

FIGURE 6-5. Measured Data for Composite Magnetic Absorber on (a) Rectangular and (b) Tapered Samples.

Appendix A

COMPUTER PROGRAM FOR NUMERICAL INVERSION OF FLAT PANEL TRANSMISSION COEFFICIENT

```
LISTING OF: &DIELC
MADE BY GAGNON.GENERAL AT  9:02 AM  TUE.,  3  DEC., 1985

00001   FTN7X
00002   c       DIELC version of 11/25/85
00003   c       This program is used to determine the complex permittivity
00004   c       of a single-layer flat panel of dielectric material from
00005   c       a measurement of the phase and amplitude of transmitted
00006   c       power through the sample for any angle of incidence. The
00007   c       program employs Muller'smethod for determining the zeroes
00008   c       of a function of a complex variable.
00009   c       ************************************************************
00010           program dielc
00011           common trans, dbeta, theta, mpol
00012           complex xg, xz, trans
00013           real eps,lamda
00014           write(1,'("ENTER ESTIMATED DIELECTRIC CONSTANT")')
00015           read(1,*)esubr
00016           xg=cmplx(esubr, 0.)
00017           nd= 7
00018           eps= 1.e-8
00019           nit= 100
00020           write(1,'("ENTER FREQUENCY IN GHZ")')
00021           read(1,*)freq
00022           freq=freq*1.e9
00023    01     write(1,'("ENTER 1 FOR PARALLEL POLARIZATION")')
00024           write(1,'("ENTER 2 FOR PERPENDICULAR POLARIZATION")')
00025           read(1,*)mpol
00026           if(mpol.ne.1 .and. mpol.ne.2) go to 1
00027           write(1,'("ENTER SAMPLE THICKNESS IN INCHES")')
00028           read(1,*) d
00029           write(1,'("ENTER INCIDENCE ANGLE IN DEGREES")')
00030           read(1,*)theta
00031           write(1,'("ENTER MEASURED PHASE SHIFT IN INCHES")')
00032           read(1,*)deltaphi
00033           write(1,'("ENTER TRANSMISSION MAGNITUDE")')
00034           read(1,*)tmag
00035           pi=atan(1.)*4.
00036           lamda=2.998e10/(2.54*freq)
00037           dbeta=d*2.*pi/lamda
00038           theta=theta*pi/180.
00039           phi=deltaphi+d*cos(theta)
00040           phi=2.*pi*phi/lamda
00041   c       trans is the measured transmission coefficient.
00042           trans=tmag*cexp((0.,-1.)*phi)
00043           call muller(xg, nd,eps,nit,  xz,iwhy)
00044           write(1,'(" ")')
00045           write(1,*)'EPSILON=',xz
00046           tandelta=-aimag(xz)/real(xz)
00047           write(1,*)'LOSS TANGENT=',tandelta
00048           if(iwhy.ne.3) go to 5
00049           write(1,'("NO CONVERGENCE!")')
00050    05     continue
00051           end
00052   c       ************************************************************
00053           subroutine muller(xg,nd,eps,nit,xz,iwhy)
```

```
00054  c
00055  c     We follow Atkinson, ''intro. to numerical analysis'' , sec. 2.10
00056  c     Recall that one is allowed to permute indices at will, sort of,
00057  c     in Newton's divided-differences. . . . . .
00058  c     fcn needed
00059  c     no deflation (only 1 zero gotten)
00060  c     input :
00061  c
00062  c     xg,      the guess at x with fcn(x)= 0.
00063  c     nd :     convergence, if nd digits agreement in two successive
00064  c              estimates of x (iwhy set to 1)
00065  c     eps :    convergence, if x found within eps (iwhy set to 2),
00066  c     nit,     the maximum number of iterations allowed (iwhy set to 3,
00067  c              if nit iterations occured without convergence)
00068  c
00069  c     output:
00070  c     xz,      the answer (if iwhy not 3)
00071  c     iwhy,    the reason it quit.  See above.
00072  c
00073        common trans, dbeta, theta, mpol
00074        complex xg,xz,  x(0:3),h, f21,f20,f01, f(0:3), f012,
00075       *   w, dent,den
00076  c
00077  c     x(3) is the new estimate, based on x0,x1,x2, with
00078  c     x(2) the old estimate
00079        real eps, epsx
00080        integer nd, nit, ic, iwhy
00081        complex fcn
00082        external fcn
00083        logical conv1
00084  c
00085        epsx = 1./10.**nd
00086        ic = 0
00087        h = (0.01, 0.)
00088        if (cabs(xg) .gt. 0.1) h=(0.1, 0.)*xg
00089        x(0)= xg-h
00090        x(1)= xg+h
00091        x(2)= xg
00092        f(0) = fcn(x(0))
00093        f(1) = fcn(x(1))
00094        f(2) = fcn(x(2))
00095        f21 = (f(1)-f(0))/(x(1)-x(2))
00096   10   continue
00097        f01 = f21
00098  c     ---------- Recall that f[x0,x1]=f[x1,x0], in Newton's world.
00099        f21 = (f(1)-f(2))/(x(1)-x(2))
00100        f20 = (f(2)-f(0))/(x(2)-x(0))
00101        w = f21 +f20 -f01
00102        f012 = (f21 - f01)/(x(2)-x(0))
00103        dent = csqrt(w*w - 4.0*f(2)*f012)
00104        if (cabs(w+dent) .ge. cabs(w-dent)) then
00105            den= w+dent
00106            else
00107            den= w-dent
00108            endif
00109        x(3) = x(2) - (2.0*f(2))/den
```

```
00110         f(3) = fcn(x(3))
00111         ic = ic+1
00112         conv1= cabs(x(3)-x(2)).le.epsx*amax1(0.01,cabs(x(3)))
00113         if (conv1.or.cabs(f(3)).le.eps .or. ic.ge.nit) go to 20
00114         x(0) = x(1)
00115         x(1) = x(2)
00116         x(2) = x(3)
00117         f(0) = f(1)
00118         f(1) = f(2)
00119         f(2) = f(3)
00120         go to 10
00121   20    continue
00122         xz = x(3)
00123         if (conv1) then
00124            iwhy=1
00125            elseif (cabs(f(3)).le.eps) then
00126            iwhy=2
00127            else
00128            iwhy=3
00129            endif
00130         return
00131         end
00132   c     ************************************************************
00133         complex function fcn(x)
00134         common trans, dbeta, theta, mpol
00135         complex x,t,trans
00136         complex radsq,rad,rpe,rpa,r,psi,psiexp
00137   c
00138   c     calculate a value for interface reflection, r, .......
00139         radsq=x-sin(theta)**2
00140         rad=csqrt(radsq)
00141         rpa=(x*cos(theta)-rad)/(x*cos(theta)+rad)
00142         rpe=(cos(theta)-rad)/(cos(theta)+rad)
00143         if(mpol.eq.1) r=rpa
00144         if(mpol.eq.2) r=rpe
00145   c     ....then calculate a value for transmission, t.
00146         psi=dbeta*rad
00147         psiexp=cexp((0.,-1.)*psi)
00148         t=(1.-r*r)*psiexp/(1.-r*r*psiexp**2)
00149   c
00150   c     fcn to be zeroed is the difference
00151         fcn=trans-t
00152         return
00153         end
```

Appendix B

ERROR MODEL FOR MULTIPLE REFLECTIONS IN THE FREE-SPACE BRIDGE DIELECTOMETER

In Figure B-1, T is the complex transmission coefficient of the system with the sample in place and is the actual measured quantity. The transmission magnitude t and transmission phase ϕ of the sample are the desired quantities for determining the sample dielectric constant and loss tangent, respectively. R is the reflection coefficient of the lens aperture of each horn, assuming they are identical. The quantity r represents the reflection from the horn feed plus any small reflections appearing down the transmission line, and γ is an unknown phase constant. The three unknowns, R, r, and γ, are determined by least-squares fit to data for transmission phase or magnitude versus separation of the two horns as measured from the micrometer-screw positioner. For the purpose of error correction, the two different reflections can actually be lumped together, greatly simplifying the model.

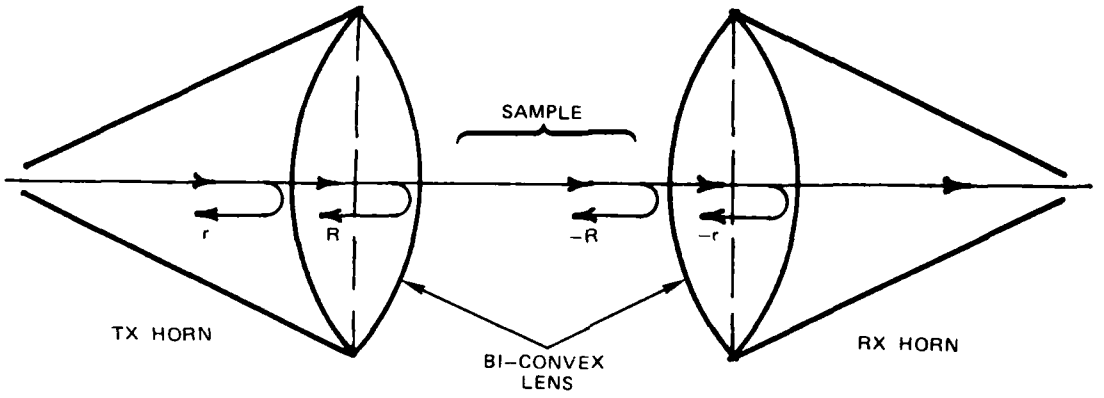

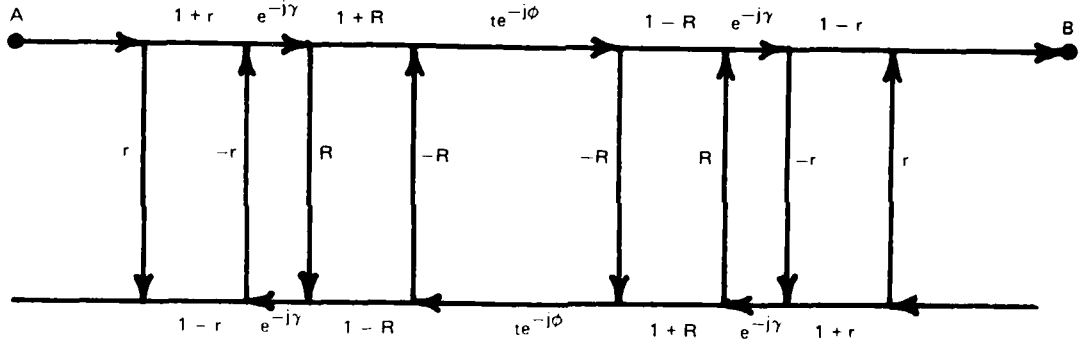

$$\bar{T} = \frac{B}{A} = \frac{(1 - r^2)(1 - R^2)\, t\, e^{-j2\gamma} e^{-j\phi}}{(1 + r R e^{-j2\gamma})^2 - (R + r e^{-j2\gamma})^2 t^2 e^{-j2\phi}}$$

$$\bar{T} = |\bar{T}| e^{-j\Phi}$$

$$\tan \Phi \approx \frac{\sin(2\gamma - \phi) - t^2 (R^2 + r^2) \sin(2\gamma + \phi) - 2r R (1 + t^2) \sin \phi}{\cos(2\gamma - \phi) - t^2 (R^2 + r^2) \cos(2\gamma + \phi) + 2r R (1 - t^2) \cos \phi}$$

$$|\bar{T}| \approx t \left[1 + 4 r R \cos 2\gamma - 2t^2 (R^2 + r^2) \cos \phi - 4 r R t^2 \cos(2\gamma - 2\phi)\right]^{-1/2}$$

FIGURE B-1. Error Model for Multiple Reflections in the Free-Space Bridge Dielectometer.

Appendix C

MULTIPLE-DIELECTRIC-SECTION INHOMOGENEOUSLY FILLED WAVEGUIDE

Composite dielectric sections in rectangular waveguides have been treated by Marcuvitz (Reference C-1) and Collin (Reference C-2). For TE_{mo} modes, the electric field is parallel to the dielectric surfaces and the propagation constant can be determined from a transverse equivalent transmission line circuit. Solutions for two- and three-dielectric sections have been obtained by this method and are shown in Figure C-1. Applied to the analysis of actual dielectric sections in waveguide, the perfect filling shown in Figure C-1 is an approximation. Gaps between the dielectric surfaces and the metallic walls and between the dielectric sections exist in laboratory realizations of these structures. Describing these "gaps" as additional dielectric sections, the ideal two- and three-section problems in Figure C-1 become five- and seven-section problems, respectively. A general solution for TE_{mo} modes with N dielectric sections is presented here. The interim sections are represented as 2 × 2 matrices combined through N-2 matrix multiplications. Whether two, three, or N sections are considered, the resulting transcendental equation must be solved numerically. The general solution has been implemented as a function subroutine requiring as input the width and dielectric constant of each section and the number of sections. Its advantage is that different dielectric section multiplicities can be analyzed with a single procedure.

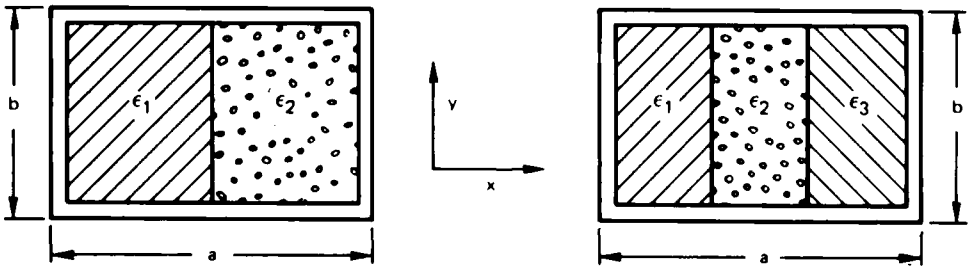

FIGURE C-1. Configuration of the Ideal Two- and Three-Section Inhomogeneously Filled Waveguides.

The N-section dielectric-filled waveguide is shown in Figure C-2.

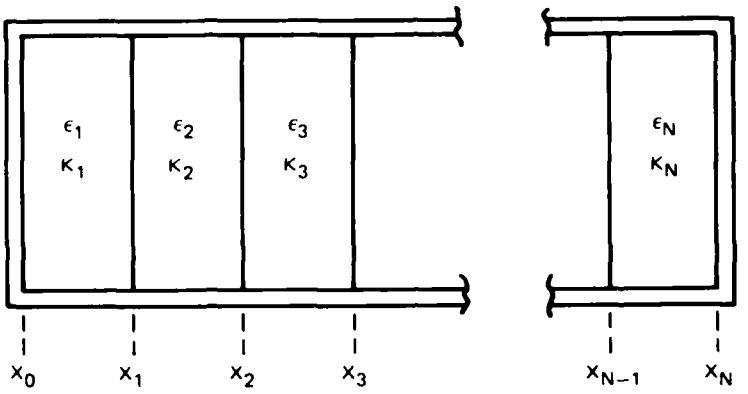

FIGURE C-2. Configuration of the N-Section Dielectric-Filled Waveguide.

Restricted to TE_{mo} modes, the electric field in the nth section can be written as

$$E_y(n) = D_n \cos k_n x + D'_n \sin k_n x \tag{C-1a}$$

where

$$k_n^2 = \epsilon_n k_0^2 - k_z^2 \tag{C-1b}$$

and

$$k_0 = \frac{\omega}{c} \quad , \quad k_z = \frac{2\pi}{\lambda_g} \tag{C-1c}$$

The quantity ϵ_n is the relative dielectric constant of the nth section. For materials with nonzero dielectric loss, $\epsilon_n = \epsilon'_n - j\epsilon''_n$. Continuity of E_y and H_z at the nth interface can be represented by

$$\hat{M}_\ell(k_n, x_n) \cdot \vec{D}_n = \hat{M}_r(k_{n+1}, x_n) \cdot \vec{D}_{n+1} \tag{C-2}$$

where $\vec{D}_n = (D_n, D'_n)^T$. The field amplitude in the 1st and nth sections are related by

$$\hat{M}_\ell(k_1, x_1) \cdot \vec{D}_1 = \{\hat{M}_r(k_2, x_1) \cdot \hat{M}_\ell^{-1}(k_2, x_2)\} \ldots$$

$$\{\hat{M}_r(k_{N-1}, x_{N-2}) \cdot \hat{M}_\ell^{-1}(k_{N-1}, x_{N-1})\}$$

$$\hat{M}_r(k_N, x_{N-1}) \cdot \vec{D}_N \qquad \text{(C-3)}$$

Defining the matrices $\hat{M}'(n)$ and $\hat{S}$ as

$$\hat{M}'(n) = \hat{M}_r(k_n, x_{n-1}) \cdot \hat{M}_\ell^{-1}(k_n, x_n) \qquad \text{(C-4a)}$$

$$\hat{S} = \hat{M}'(2) \cdot \hat{M}'(3) \ldots \hat{M}'(N-1) \qquad \text{(C-4b)}$$

the field amplitude relations become

$$\hat{M}_\ell(k_1, x_1) \cdot \vec{D}_1 = \hat{S} \cdot \hat{M}_r(k_N, x_{N-1}) \cdot \vec{D}_N \qquad \text{(C-4c)}$$

The components of $\hat{M}'(n)$ are

$$\hat{M}'(n) = \begin{bmatrix} \cos k_n(x_n - x_{n-1}), & -k_n^{-1} \sin k_n(x_n - x_{n-1}) \\ k_n \sin k_n(x_n - x_{n-1}), & \cos k_n(x_n - x_{n-1}) \end{bmatrix} \qquad \text{(C-5)}$$

The electric fields are null at the metallic boundaries x_0 and x_N and give the conditions

$$\hat{M}_r(k_N, x_{N-1}) \cdot \vec{D}_N = \begin{bmatrix} \sin k_N(x_N - x_{N-1}) \\ - k_N \cos k_N(x_N - x_{N-1}) \end{bmatrix} D(N) \qquad \text{(C-6a)}$$

and

$$\hat{M}_\ell(k_1, x_1) \cdot \vec{D}_N = \begin{bmatrix} - \sin k_1(x_1 - x_0) \\ - k_1 \cos k_1(x_1 - x_0) \end{bmatrix} D(1) \qquad \text{(C-6b)}$$

where D(N) and D(1) are scalars. Substituting into Equation C-4c gives two equations in D(N) and D(1). A nontrivial solution requires

$$\frac{S_{21}}{k_1 k_N} \sin k_1(x_1 - x_0) \sin k_N(x_N - x_{N-1})$$

$$+ S_{12} \cos k_1(x_1 - x_0) \cos k_N(x_N - x_{N-1})$$

$$- \left[\frac{S_{22}}{k_1} \sin k_1(x_1 - x_0) \cos k_N(x_N - x_{N-1}) \right.$$

$$\left. + \frac{S_{11}}{k_N} \cos k_1(x_1 - x_0) \sin k_N(x_N - x_{N-1}) \right] = 0 \qquad \text{(C-7)}$$

Equation C-7 represents the general solution for the N-section problem.

The general solution can be represented more compactly. Defining $T_n = \tan k_n(x_n - x_{n-1})$, the general transcendental equation becomes

$$S_{21} \frac{T_1 T_N}{k_1 k_N} - \left[S_{22} \frac{T_1}{k_1} + S_{11} \frac{T_N}{k_N} \right] + S_{12} = 0 \qquad \text{(C-8)}$$

Since

$$\hat{M}'(n) = \begin{bmatrix} 1 & -T_n/k_n \\ k_n T_n & 1 \end{bmatrix} \qquad \text{(C-9)}$$

for numerical calculations, the matrix of a section (Equation C-9) is determined and multiplied by S, producing the new value of S (Equation C-4). This procedure is repeated for each of the N-2 interior sections. The results are substituted into the "function" (Equation C-8). Zeros of Equation C-8 and thus solutions are determined using standard numerical techniques. In practice, the functional form of Equation C-7 is used, avoiding the numerical problems associated with poles in the tangent functions.

Applying the general result of Equations C-8, C-4, and C-9 to the two-, three-, and four-section problems gives

Two Sections

$$\frac{T_1}{k_1} + \frac{T_2}{k_2} = 0$$

Three Sections

$$\frac{T_1 T_3}{k_1 k_3} [k_2 T_2] - \left[\frac{T_1}{k_1} + \frac{T_2}{k_2} + \frac{T_3}{k_3} \right] = 0$$

Four Sections

$$\frac{T_1 T_4}{k_1 k_4} (k_2 T_2 + k_3 T_3) + \frac{T_4}{k_4} \left(\frac{k_3}{k_2} T_2 T_3 \right) + \frac{T_1}{k_1} \left(\frac{k_2}{k_3} T_2 T_3 \right)$$

$$- \left[\frac{T_1}{k_1} + \frac{T_2}{k_2} + \frac{T_3}{k_3} + \frac{T_4}{k_4} \right] = 0$$

The symmetrical three-section solution $\varepsilon_1 = \varepsilon_3$, $x_3 = a$, and $x_2 - x_1 = d$ gives

$$\left[\frac{1}{k_1}\tan k_1\left(\frac{a-d}{2}\right) - \frac{1}{k_2}\cot\frac{k_2 d}{2}\right] \cdot \left[\frac{1}{k_1}\tan k_1\left(\frac{a-d}{2}\right) + \frac{1}{k_2}\tan\frac{k_2 d}{2}\right] = 0$$

The antisymmetric solution (tan, tan) differs by a sign from the result given by Collin (Reference C-3).

As noted at the beginning of this section, the general solution (Equation C-8) is readily implemented numerically as a single procedure, which makes explicit expressions for the cases of different multiplicities unnecessary. It should also be noted that as the frequency is increased above cutoff, at some point the angle of incidence for a particular layer will exceed the critical angle in propagating from a higher dielectric material to a lower one (Reference C-4). This leads to total internal reflection. In such a case, an evanescent wave exists in the lower dielectric constant material, and the tangent function in Equation C-8 becomes a hyperbolic tangent. Further complexity results in lossy materials caused by the fact that real and imaginary characteristic equations must be solved simultaneously.

REFERENCES

C-1. N. Marcuvitz. Waveguide Handbook. Lexington, Mass., Boston Technical Publishers, Inc., 1964. Vol. 10, MIT Radiation Laboratory Series, Chap. 8.

C-2. Robert E. Collin. Field Theory of Guided Waves. New York, McGraw-Hill, 1960. Chap. 6.

C-3. -----. P. 288 (Equations 9a and 9b).

C-4. D. J. White and G. Everett. "Adding Plane Waves to Find the Complete TM and TE Wave Solutions for Metallic Rectangular Waveguide," Am. J. Phys., Vol. 51, No. 12 (December 1983), pp. 1115-19.

Appendix D

BALANCED MIXER MAGNITUDE ERRORS: DEVIATIONS FROM SQUARE-LAW RESPONSE

Analysis of data obtained with a moving vane dielectometer system exhibits magnitude errors that cannot be attributed to the finite reflection coefficients of the microwave system components used. The spectral purity of the power source was measured and is not the source of these errors. Detector crystal square-law deviations become the major error source when used with a nearly ideal circulator.

The moving vane dielectometer is computer controlled. Data are obtained as follows: For the phase shifter in the mixer reference arm, set first at 0 degree then at 90 degrees; the in-phase and quadrature variations versus vane position are determined and stored as disk files. The position dependence of the magnitude and phase of the reflection coefficient are computed. Data obtained for a moving short at 9.7 gigahertz are shown in Figure D-1. In the absence of system errors, the magnitude should be a constant.

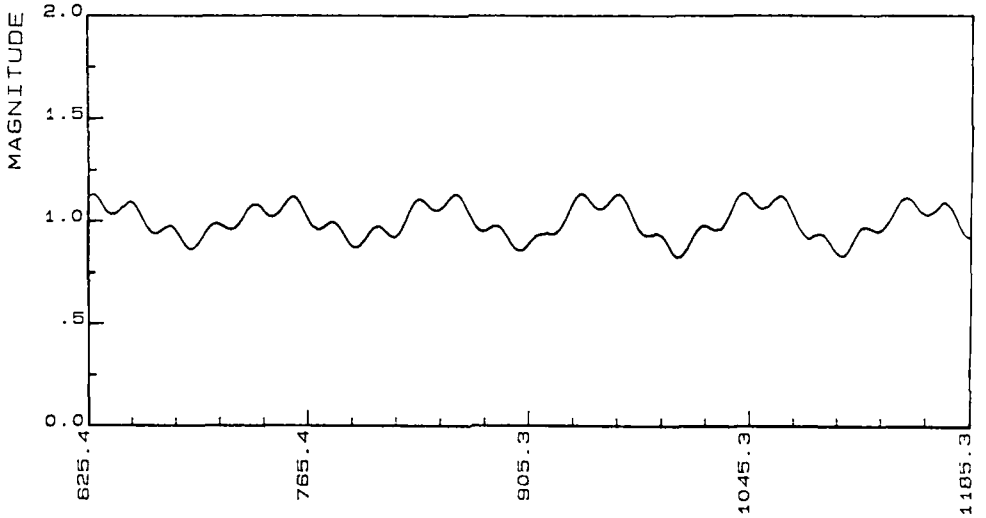

FIGURE D-1. Measured Magnitude Variation of the Voltage Reflection Coefficient for a Moving Short in the Waveguide; Nonideal Bahavior.

The microwave circuit (Figure 6-2) has been analyzed. Nonideal circulator response is represented by (T_{22}, $T_{13} \neq 0$) in the response matrix T. The output of the mixer is represented by

$$e_m = \left\{\left(1 + \frac{1}{2}\epsilon\right)\left|E_S + E_R\right|^{2+\eta_1} - \left(1 - \frac{1}{2}\epsilon\right)\left|E_S - E_R\right|^{2+\eta_2}\right\} \qquad (D\text{-}1)$$

where E_S and E_R represent the electric fields (complex) from the "signal"; η_1 and η_2, the mixer crystal square law deviation; and ϵ, crystal unbalance.

The "apparent" magnitude of the moving short reflection coefficient has been calculated numerically and is plotted versus the phase (relative position) of the reflection coefficient with no system errors.

Figure D-2 shows the behavior of parameters that represent the general form of the experimentally measured variation (Figure D-1) and corresponds to

$$T_{22} = 0.02, -45°, \; T_{13} = 0$$

$$(\eta_1, \eta_2) = -0.2$$

$$\epsilon = 0.01$$

From data obtained with a moving short, the parameters characterizing the square-law deviations of the mixer crystals can be determined using conventional numerical curve-fitting techniques. Alternately, the measured moving short response, tabulated as magnitude versus phase, can be used directly to correct system errors. The power level dependence of square-law deviations requires the use of identical average powers at the mixer. Clearly preferable to this approach is a power decrease, so that square-law deviations are both minimized and become insensitive to small power changes.

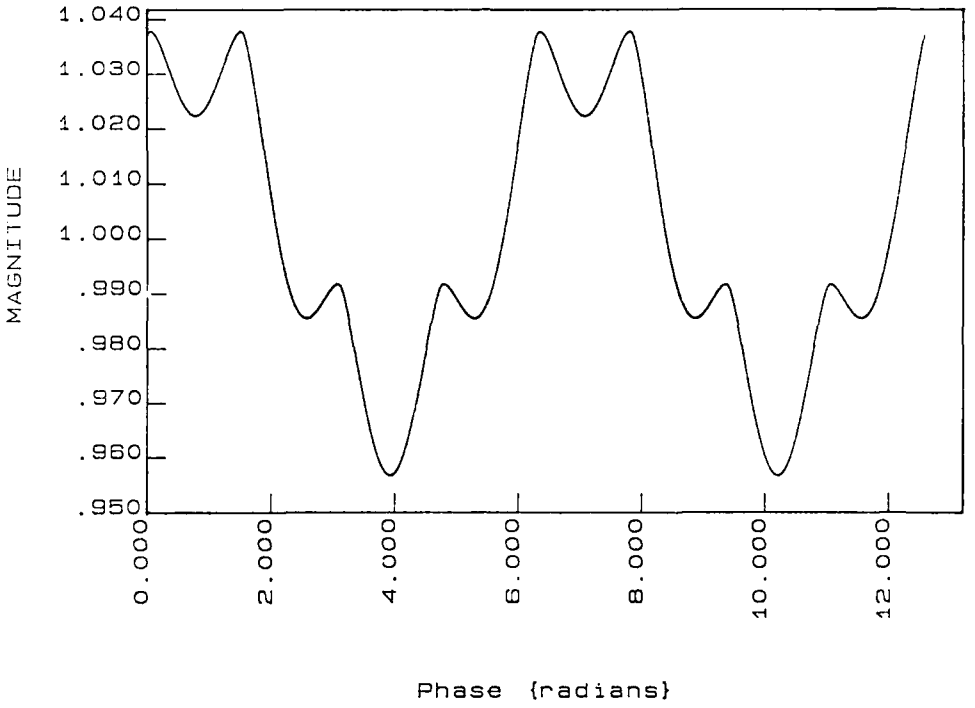

FIGURE D-2. Calculated Variation of the Voltage Reflection Coefficient for a Moving Short in the Waveguide.

INITIAL DISTRIBUTION

3 Naval Air Systems Command
- AIR-310B, D Mulville (1)
- AIR-723 (2)

2 Chief of Naval Research, Arlington
- ONR-414
  - K. Davis (1)
  - M. Morgan (1)

3 Naval Sea Systems Command
- SEA-09B312 (2)
- SEA-62R41 (1)

1 Commander in Chief, U. S. Pacific Fleet (Code 325)
1 Commander, Third Fleet, Pearl Harbor
1 Commander, Seventh Fleet, San Francisco
2 Naval Academy, Annapolis (Director of Research)
1 Naval Air Development Center, Warminster
- Code 60613, H. Lee (1)
- Code 606A, A. Fletcher (1)

4 Naval Research Laboratory
- Code 6360
  - W. McDonough (1)
  - R. Rice (1)
- C. Carasella (1)
- F. Rachford (1)

3 Naval Ship Weapon Systems Engineering Station, Port Hueneme
- Code 5711, Repository (2)
- Code 5712 (1)

1 Naval Surface Weapons Center, Dahlgren (Code G23, C. Blackmon)
2 Naval Surface Weapons Center, White Oak Laboratory, Silver Spring
- Code K-22
  - G. Matteson (1)
  - W. Messick (1)

1 Naval War College, Newport
4 Office of Naval Technology, Arlington
- OCNR-213, D. Siegel (1)
- OCNR-225, M. Kinna (1)
- ONR-11, A. Dinnes (1)
- ONR-1131, R. Pohanka (1)

2 Army Missile Command, Redstone Arsenal
- AMSMI-RLA, K. Letson (1)
- DRSMI-RLM, P. Ormsby (1)

4 Air Force Armament Laboratory, Eglin Air Force Base
- AFATL DLC (1)
- AFATL DLCA (1)
- AFATL DLCM (1)
- AFATL DLCV (1)

1 Air Force Intelligence Service, Bolling Air Force Base (AFIS/INTAW, Maj. R. Lecklider)
2 Air Force Wright Aeronautical Laboratories, Wright-Patterson Air Force Base
- AFWAL/AADM, A. E. Blume (1)
- AFSC, Maj. J. Speers (Materials Laboratory) (1)

1 Arnold Engineering Development Center, Arnold Air Force Station, (Maj. R. Bowman)

END

DTIC

6-86